soil systems

MDPI

Article

Hot Spots and Hot Moments of Soil Moisture Explain Fluctuations in Iron and Carbon Cycling in a Humid Tropical Forest Soil

Diego Barcellos [1], Christine S. O'Connell [2], Whendee Silver [2], Christof Meile [3] and Aaron Thompson [1,*]

1 Department of Crop and Soil Sciences, University of Georgia, Athens, GA 30602, USA; diego.barcellos@yahoo.com.br
2 Department of Environmental Science, Policy, and Management, University of California-Berkeley, Berkeley, CA 94720, USA; coconn@berkeley.edu (C.S.O.); wsilver@berkeley.edu (W.S.)
3 Department of Marine Sciences, University of Georgia, Athens, GA 30602, USA; cmeile@uga.edu
* Correspondence: aaront@uga.edu; Tel.: +1-706-410-1293

Received: 30 September 2018; Accepted: 27 October 2018; Published: 1 November 2018

Abstract: Soils from humid forests undergo spatial and temporal variations in moisture and oxygen (O_2) in response to rainfall, and induce changes in iron (Fe) and carbon (C) biogeochemistry. We hypothesized that high rainfall periods stimulate Fe and C cycling, with the greatest effects in areas of high soil moisture. To test this, we measured Fe and C cycling across three catenas at valley, slope, and ridge positions every two days for a two-month period in a rainforest in Puerto Rico. Over 12 days without rain, soil moisture, Fe^{II}, rapidly reducible Fe oxides (Fe^{III}_{RR}), and dissolved organic C (DOC) declined, but Eh and O_2 increased; conversely, during a 10-day period of intense rain (290 mm), we observed the opposite trends. Mixed-effects models suggest precipitation predicted soil moisture, soil redox potential (Eh), and O_2, which in turn influenced Fe reduction/oxidation, C dissolution, and mineralization processes. The approximate turnover time for HCl-extractable Fe^{II} was four days for both production and consumption, and may be driven by fluctuations in Fe^{III}_{RR}, which ranged from 42% to 100% of citrate–ascorbate-extractable Fe^{III} (short-range order (SRO)-Fe^{III}) at a given site. Our results demonstrated that periods of high precipitation (hot moments) influenced Fe and C-cycling within day-to-week timescales, and were more pronounced in humid valleys (hot spots).

Keywords: iron reduction; dissolved organic carbon; soil moisture; redox processes

1. Introduction

Rainfall infiltrates into the soil, changing soil moisture and oxygen (O_2) concentrations, and substantially modifying the soil biogeochemical processes that govern carbon (C) and iron (Fe) cycling. These processes have important implications for land management and the soil's response to a changing climate [1–4]. In humid tropical regions, rainfall can be very high, with annual averages ranging from 3 m to 10 m (e.g., the Caribbean and Amazon forests) [5–7]. High rainfall accelerates soil genesis by rapidly removing reaction products and maintaining a moist environment for microbial activity, which ultimately results in the accumulation of Fe and Al oxides at the expense of other minerals [8,9]. Rainfall patterns directly influence soil moisture content [10], which can govern C and nutrient biogeochemical cycling and mineral–organic associations and, together with pH, modulate the net primary productivity (NPP) of ecosystems [1].

Variations in soil moisture can lead to changes in O_2 concentrations across the landscape [11], influencing elements sensitive to reduction/oxidation (i.e., redox) reactions, such as nitrogen, manganese, iron, sulfur, and carbon [12,13]. Iron oxyhydroxides are particularly important in soils

from humid tropical regions, as Fe often becomes the most utilized terminal electron acceptor when O_2 is depleted, and the reductive dissolution of Fe minerals can release sorbed nutrients and C [14–16]. With enough labile C and active microorganisms, fluctuating soil moisture and O_2 can generate pockets of anoxic conditions, even in well-drained upland soils, creating "slope wetlands" [17]. Changes in soil redox status can stimulate Fe cycling by repeatedly forming low-crystallinity or short-range order (SRO) Fe^{III} phases, some of which—below referred to as $Fe^{III}{}_{RR}$—are rapidly reducible by microorganisms during anaerobic conditions [18]. Other portions of the SRO Fe^{III} pool, along with more crystalline Fe^{III} phases, such as hematite or well-crystalline goethite, supply electron-accepting capacity over longer timescales [19,20]. Thus, assessing shifts in the pools of reduced (Fe^{II}) and rapidly-reducible ($Fe^{III}{}_{RR}$) iron phases are important for predicting soil biogeochemical processes that intersect with Fe cycling.

Soils experiencing spatial and temporal variation in moisture and O_2 content may exhibit different rates of Fe reduction, and thus the dissolution of solid-phase C. Carbon is often bound to Fe phases and can be released as dissolved organic carbon (DOC), which then may stimulate microbial respiration and emissions of CO_2 and CH_4 [21–26]. In addition, during the oxidation of $Fe^{2+}{}_{(aq)}$, Fenton reactions can produce OH radicals and drive additional DOC loss or CO_2 production [27–29]. The oxidation of Fe^{II} can also facilitate the formation of Fe^{III} phases that can co-precipitate with DOC or serve as sorbents for DOC [30]. Soil organic matter is often associated with Fe minerals in humid tropical ecosystems [31–34], and these mineral–organic associations can account for up to 80% of the total C stocks in mineral soils with low particulate organic matter [35].

Much of our understanding of the coupling of Fe–C biogeochemical processes derives from laboratory incubation studies; in contrast, detailed field measurements of short-term (days–weeks) shifts in Fe dynamics are lacking. The rapid fluctuations in soil moisture and O_2 content [36] can create hot moments of anoxic soil microsites that facilitate Fe reduction and C decomposition [37]. However, the repeated soil sampling that is necessary to identify this phenomenon in the field is rarely conducted. Spatially, topographic positions (i.e., ridges, slopes, and valleys) often exhibit distinct hydrological and geomorphological characteristics that respond differently to water drainage or accumulation [38], leading to distinct hot spots throughout the landscape. For example, soils from the Luquillo Experimental Forest (LEF) in Puerto Rico exhibited Fe^{II} concentrations varying from 22 mmol to 212 mmol of Fe^{II} per kg of dry soil over different landscape positions and along an elevation gradient [35]. Thus, redox processes likely proliferate in hot spots, and at specific hot moments across the landscape where and when biogeochemical reaction rates are more rapid [39–41].

We aimed to capture hot moments (of hours to days) of Fe reduction associated with C decomposition and redox processes across different topographic positions (ridge, slopes, valleys) that could serve as hot spots in the landscape. We hypothesized the following. (1) Rainfall events will alter soil moisture and O_2 within hours to days, increasing Fe reduction rates, organic C mineralization, and DOC release, with rapid changes in redox potential (constituting hot moments). (2) These hot moments will occur more rapidly and persist longer in valley topographic positions (hot spots) and will lead to greater rates of Fe redox transformations associated with C cycling. We also sought to assess the HCl-extractable Fe^{II} turnover times in these humid tropical forest soils. To test these hypotheses, we collected triplicated soil samples over a two-month period from three topographic positions (valley, slope, and ridge) every two to three days from three replicated catenas in a montane forest in Puerto Rico (USA). Measurements included bulk soil extractions of Fe^{II}, DOC, pH, gravimetric water content, and soil incubations to measure the potential for Fe reduction and the availability of rapidly reducible Fe^{III} oxides. In addition, we monitored soil redox potential (Eh), soil O_2, volumetric water content, and CO_2 and CH_4 fluxes. Relationships among these measurements were then analyzed using multivariate statistical techniques (repeated measures).

2. Materials and Methods

2.1. Site Description, Experimental Design, and Soil Sampling Procedure

We sampled soils from three topographic positions (ridge, slope, and valley) across three replicated catenas (Figure S1) from May to June of 2016 near the El Verde Field Station (University of Puerto Rico, Río Piedras) (Figure S2) in the Luquillo Experimental Forest (LEF). The studied sites are in the Espíritu Santo watershed, part of the NSF-sponsored Luquillo Critical Zone Observatory (LCZO) and Long-Term Ecological Research (LTER) programs. The parent material is predominantly volcanoclastic rocks derived from Cretaceous andesitic magma [42,43]. Mean annual precipitation is ~3500 mm y^{-1} varying from 2600 y^{-1} to 5800 mm y^{-1}, and characterized by low seasonality, but including extreme rainfall events (as high as 100 mm d^{-1}) associated with Caribbean storm systems [44]. The dominant tree species in this part of the LEF is the Tabonuco (*Dacryodes excelsa*).

The catenas form steep and convex–concave hillslopes draining to ephemeral streams that are characterized by heterogeneous soil distribution and microsites across ridges, slopes, and valleys [45]. Catena-1 is relatively small, with about 5 m of vertical rise, a steep slope, a gentle ridge, and valley usually characterized by high soil moisture—Global Positioning System (GPS) coordinates in Table S1). Catena-2 is in another hillslope, about 80 m apart from Catena-1, with 20 m of vertical rise, containing a spine ridge, a steep and long slope, and a valley that is occasionally flooded with water. Catena-3 is downstream of Catena-1, in the same hillslope, with a vertical rise of 10 m, a steep slope, a gentle ridge, and thus similar to Catena-1 except that the valley in Catena-3 is not as saturated as Catena-1. Catena-1 was previously studied by O'Connell, Ruan and Silver [36] and Catena-3 was studied by Almaraz [46]. The hillslope hydrology is characterized by valleys constantly receiving water and sediments from upper slope and ridge positions via runoff or lateral movement of water within the soil. Typically, the soils in the Tabonuco forest are Ultisols (Typic Haplohumults) in stable ridges, Oxisols (Inceptic and Aquic Hapludox) in the slopes, and predominately Inceptisols (Typic Eutrudepts) in the valleys [35].

We studied a total of nine sites, with three located on ridges, slopes, and in valleys, respectively. For each sampling site, we allocated three replicate plots of 1.5 m × 1.5 m for soil sampling (Figure S1). Triplicate composite soil samples from each site were taken within plots for chemical characterization. We sampled soils from the top 15 cm, using a 1-cm diameter soil probe, and each soil sample was taken at least 20 cm apart from the previous sampling spots (Figure S1). Soil samples were placed in polypropylene bags within a cooler, and analysis (described below) began at the El Verde Field Station within 20 min of sampling. Samples were taken every two to three days, except when a lack of power in the field station prevented sample processing (for example, from 6 May 2016 to 14 May 2016). We collected soil samples a total of 17 times during the experimental time span of 44 d. The rainfall dataset was acquired from the rainfall gauge collected daily at the El Verde Field Station, which is available on the website of the Luquillo Long-Term Ecological Research Program (https://luq.lter.network/data). Collection procedures are described in McDowell and Estrada-Pinto [47].

2.2. Soil Biogeochemical Characterization and Extractions (Measurements within Days)

We conducted a series of bulk biogeochemical characterization tests from the triplicated samples including: measurements of HCl-extractable ferrous iron (Fe^{II}), water-extractable dissolved organic carbon (DOC), pH, and gravimetric water content (θ_G); an assessment of rapidly-reducible Fe oxides (abbreviated as $Fe^{III}{}_{RR}$); and on select random samples from the archive, we made general soil characterizations (including Fe and C pools, and soil texture).

Ferrous iron (Fe^{II}) was determined by extraction with 0.5 M of HCl at a 1:10 soil:solution ratio (50 mg of soil), by shaking for two hours (horizontal shaker), and centrifuging for 10 min at 11,000 Relative Centrifugal Force (RCF) [48]. The supernatant was taken, and Fe^{II} was analyzed by the colorimetric ferrozine method, according to Barcellos, et al. [49] and Thompson, et al. [50] with the 562-nm and 500-nm intensities measured in 96-well microplates [51] using a portable Tecan Infinite F50 plate reader.

Water-extractable dissolved organic carbon (DOC) was obtained by extraction at 1:5 soil:deionized (DI) water ratio (2 g of soil) and shaking for 1 h in a horizontal shaker at room temperature [52–54]. The suspension was centrifuged for 15 min at 4600 RCF, and the supernatant was filtrated with 0.70-µm glass fiber filters [55]. Filtered supernatants were immediately frozen at −20 °C and then shipped to the University of Georgia at the end of the field session and analyzed on a Shimadzu 5050 TOC analyzer.

Soil pH was measured in 1:1 soil:DI-water ratio (5 g of soil) using an Orion Ross sure-flow pH electrode. Gravimetric water content (θ_G) was determined by oven-drying soils for >24 h and reporting the as dry-weight basis. Composite samples selected from random days of sampling (over 10 samples) were pooled (100 g of soil) and analyzed in triplicate for the following: total elemental analysis by lithium borate fusion prior to acid dissolution followed by ICP-MS analysis, short-range order (SRO) Fe by 0.2 M of sodium citrate/0.05 M of ascorbic acid extraction followed by ICP-MS analysis, total carbon and nitrogen measured in a CHN Carlo Erba Elemental Analyzer, and soil texture determined by a Beckman Coulter LS 13 320 Laser diffraction Particle Size Analyzer [56]. Soils were not sampled for catena-3 on 13 June 2016. We additionally archived soil samples from each sampling time-point and site, and stored ~15 g soil (frozen at −20 °C) for future analysis.

Rapidly-Reducible Fe Oxides (Fe^{III}_{RR}) Microbial Bioreduction Assay

We quantified the amount of rapidly-reducible ferric iron (Fe^{III}_{RR}) using microbial bioreduction assays adapted from Ginn, Meile, Wilmoth, Tang and Thompson [18] to work at the field station using the field-moist fresh soils. Microbial bioreduction assays have been used in other studies to assess the soil's potential for Fe reduction [18,57–59]. We conducted two different assays. In the first, a *Shewanella oneidensis* MR-1 culture along with a growth medium [18] (see below) was added to the soil (abbreviated as Shewa-Fe^{III}_{RR}), while in the second, the native soil was incubated with growth media only (abbreviated as Media-Fe^{III}_{RR}). This assessed the availability of the soil Fe^{III} phases for Fe reduction by the indigenous microbial communities when appropriate nutrients and C were provided, while the addition of the Fe-reducer *Shewanella* sp. aimed at overcoming microbial limitations.

For the Shewa-Fe^{III}_{RR} treatment, *Shewanella oneidensis* MR-1 was grown to the late exponential and early stationary phase in a selective media containing 0.5 g L^{-1} of KH_2PO_4, 1.0 g L^{-1} of $NaSO_4$, 2.0 g L^{-1} of NH_4Cl, 1.0 g L^{-1} of yeast extract, 0.5 mM of $CaCl_2$, 0.1 mM of $MgSO_4$, 10 mM of Na-lactate, and 50 mM of Fe-citrate (adapted from Ginn, Meile, Wilmoth, Tang and Thompson [18]). Cell densities were obtained by optical density measurements at a wavelength of 660 nm that had been previously calibrated by a direct count of cells using epifluorescence microscopy to reach a population density of over 10^8 CFU mL^{-1} [58]. After *S. oneidensis* growth, we conducted a washing procedure twice, by first centrifuging the cells at 3000 RCF for 30 min, discarding the supernatant, and adding a new fresh selective media with the same composition as above, but without yeast extract or Fe-citrate, and then re-doing the centrifugation procedure and disposing the supernatant [18]. In sequence, we added the fresh collected soil with the washed bacterial culture suspended in new fresh selective media (same composition, without yeast extract or Fe-citrate), at a ratio of 1:10 soil:media, in a gas tight tube. In parallel, for the Media-Fe^{III}_{RR} treatment, we added the fresh soil to the fresh selective media above (without yeast extract or Fe-citrate) and with no *S. oneidensis*, and placed them in similar gas tight tubes, at a ratio of 1:10 soil:media. For both Shewa-Fe^{III}_{RR} and Media-Fe^{III}_{RR}, we flushed the tube headspace with inert N_2 gas to create anoxic conditions and placed it on an end-over-end shaker for 7 d in the dark. After 7 d of incubation, we pipetted 0.5 mL of either Shewa-Fe^{III}_{RR} or Media-Fe^{III}_{RR} suspension treatments, centrifuged at 11,000 RCF for 30 min, removed the supernatant, and then revolved and extracted the pellet with 0.5 M of HCl for 2 h to obtain Fe^{II} concentrations using the ferrozine protocol described above. Results were expressed in mmol Fe kg^{-1} d^{-1} (iron reduction rates), on a dry soil mass basis by calculating the difference in Fe^{II} concentrations between day 0 and 7 of the incubation.

2.3. Soil Sensors and Data Collection (Measurements within Hours)

For each site within each of the three catenas, we deployed four platinum electrodes (Paleo Terra Inc., Amsterdam, The Netherlands) adjacent to the plots (Figure S1) measuring the redox potential (Eh) every minute and storing the data every hour via CR23X Campbell data loggers. Measurements of Eh recorded the voltage difference between the reference electrode and a redox electrode (Pt sensor). The Pt sensor was placed for Eh readings at 7.5 cm depth from the soil surface. Eh values (normalized to pH 7, Eh_7) serve as a proxy for four major redox conditions in soils: Eh_7 values over +400 mV indicate oxidizing conditions (aerated soils), Eh_7 values between +100–400 mV indicate moderately reducing conditions, Eh_7 values between −100 and +100 mV indicate reducing conditions, and Eh_7 values below −100 mV indicate highly reducing (anoxic) conditions [60–62]. Eh_7 values around +300 mV can be considered the boundary between aerobic and anaerobic conditions [63].

At catena-1 only, volumetric water content (θ_V), soil oxygen content (O_2), and fluxes of CO_2 and CH_4—denoted F(CO_2) and F(CH_4)—were measured near the ridge, slope, and valley sampling plots [36]. Time-domain reflectometry (TDR) probes were used to track volumetric water content, and galvanic Apogee O_2 sensors encapsulated in polyvinyl chloride (PVC) chambers were used to track soil O_2 concentrations [37]. For each site in catena-1, we deployed five TDR and five O_2 sensors installed in the top 15 cm of the soil, and data was stored every hour in CR1000 Campbell dataloggers. Emissions of CO_2 and CH_4 were measured using automated flux chambers deployed in each site (three for the valley, three for the slope, and three for the ridge). Gases were collected within the chambers over 10 minutes of sampling, three minutes of flushing between measurements, and automatically transported to a cavity ring down spectroscopy (CRDS) gas analyzer (Picarro, Santa Clara, CA, USA) within the site [36]. Gas samples were collected daily at a maximum of 12 samplings per day per chamber with F(CO_2) expressed in μmol m^{-2} s^{-1} and F(CH_4) in nmol m^{-2} s^{-1}.

2.4. Statistical Analyses

The soil characteristics (SRO-Fe, Total-Fe, Total-C, and soil texture) in Table 1 were analyzed using one-way ANOVA followed by Tukey's HSD (honestly significant difference) test at the 5% probability level in R. We computed models using the daily average for the environmental factors (Eh, O_2, and θ_V, measured by sensors) and the daily average precipitation to predict the drivers for Eh, O_2, and θ_V (see initial parameters in Table S4), using the lmer function from the lme4 package in R [64]. We also computed turnover times for the HCl-extractable Fe^{II} pool (for both production and consumption) by dividing the Fe^{II} concentration by the change of Fe^{II} with respect to time between two subsequent sampling points $\left(\tau = \left(\frac{Fe^{II}_{sample\ 1} + Fe^{II}_{sample\ 2}}{2}\right) / \left(\frac{Fe^{II}_{sample\ 2} - Fe^{II}_{sample\ 1}}{t_{sample\ 2} - t_{sample\ 1}}\right)\right)$, for an average of all of the sites, as well as for each site individually. We plotted the HCl-extractable Fe^{II} turnover times in histograms and reported the most commonly occurring, the mean, and the median turnover time, respectively.

We analyzed the relationship between the biogeochemical measurements using a linear mixed model fit by restricted maximum likelihood (REML), for the sampling days and within the different topographic positions (and sites) of the catenas using the lmer function from the lme4 package in R [64]. The outcome variables that were considered included Fe^{II}, $Fe^{III}{}_{RR}$ (Media or Shewa), DOC, and Eh. We additionally ran models just for catena-1 to assess relationships between our measurements and the additional sensor measurements (O_2, θ_V) and CO_2 and CH_4 fluxes that were only measured in catena-1. We used a dataset with 17 days of observation spread across 44 days. Predictor variables included DOC, Media-$Fe^{III}{}_{RR}$, pH, θ_G, precipitation, and in the case of catena-1, also O_2 and θ_V (replacing θ_G).

We surmised that the Fe and C cycling may not respond immediately by changes in precipitation, Eh, O_2, and θ_V, but instead may exhibit a lag (of hours/days) before responding. Thus, we averaged each of these continuously measured variables over different windows of time prior to the time of sampling, and then used a procedure of minimizing Akaike's information criterion (AIC) to select the optimum model (lowest AIC). For precipitation, we compared the averages of one day, two days, three days, four days, five days, and 10 days prior to soil sample collection, and choose the one with the

lowest AIC (two-day lag; precipitation_48 h). For the Eh, O_2, and θ_V sensors, we compared the AIC at the hour in which the soil sample was taken, and for the average of these sensor readings in the last 2 h, 3 h, 6 h, 12 h, 24 h, 36 h, and 48 h before the soil sampling. For example, for a soil sample taken at 14:00 on 14 May 2016 (day 10), we averaged the Eh measurement at 14:00 (Eh_1 h), and then from 13:00 to 14:00 (Eh_2 h), 12:00 to 14:00 (Eh_3 h), and so on until 48 h prior to the measurement. We reported both AIC and R^2 of the models calculated by r.squaredGLMM from the R package MuMIn for generalized linear mixed effects models (GLMMs) [65,66] in order to compare the models.

Table 1. Summary of soil characterization for each catena and topographic position: mean (±1 standard error). Lowercase letters (a, b, c, d) indicate significant differences among the variables by ANOVA and Tukey's HSD test at the 5% probability level. Soils from the Luquillo Experimental Forest (LEF), Puerto Rico, sampled in 2016. SRO: short-range order.

Site	SRO-Fe † mmol kg^{-1}	Total-Fe mmol kg^{-1}	Carbon (%)	Clay (%)	Sand (%)	Silt (%)	pH ‡
Valley-1	336 (32) a	1162 (10) a	4.6 (0.1) a	7 (0.6) a	45 (3.6) a	48 (1.9) a	6.1 (0.2) a
Valley-2	305 (21) a	1353 (12) b	4.0 (0.2) a	8 (0.7) a	36 (2.7) a	56 (2.1) b	5.3 (0.2) b
Valley-3	195 (10) b	1409 (14) c	3.1 (0.1) b	10 (0.9) b	33 (2.6) b	56 (2.3) b	5.3 (0.1) b
Slope-1	178 (10) b	1403 (12) c	3.4 (0.3) b	10 (0.6) b	27 (3.4) b	63 (2.0) c	5.1 (0.2) bc
Slope-2	213 (7) b	1503 (13) d	3.1 (0.1) b	12 (1.1) b	28 (2.2) b	60 (2.4) c	4.8 (0.2) d
Slope-3	131 (11) c	1434 (12) c	3.4 (0.1) b	8 (0.2) a	45 (1.0) a	47 (0.8) a	5.1 (0.1) bc
Ridge-1	190 (17) b	1428 (12) c	4.5 (0.4) a	6 (0.4) a	43 (4.2) a	51 (1.7) a	4.9 (0.2) d
Ridge-2	227 (9) b	1334 (13) b	5.9 (0.1) c	5 (0.5) a	52 (2.6) ad	43 (2.2) a	4.8 (0.2) d
Ridge-3	206 (6) b	1340 (12) b	4.6 (0.1) a	5 (0.4) a	60 (4.8) cd	36 (1.4) d	5.0 (0.2) cd

† Citrate-Ascorbate Extraction. ‡ pH average for all 17 days of soil collection.

3. Results

3.1. Soil Characteristics across Sites

Soil characteristics (Table 1) varied along the replicated topographic positions. Valley-1 and -2 had the highest SRO-Fe among all of the samples (Table 1). Even with the lowest total-Fe, valley-1 had the highest amount of reactive iron (SRO-Fe) and ferrous iron (Fe^{II}) of all of the sites (Table 1). Total-C was high in valley-1 and -2 and in the ridges, compared to the slopes; thus, there was more C accumulation in the valleys and ridges compared to the slopes (Table 1). Soils had a loam texture for most of the sites, or sandy loam and silt loam for a few sites (Table 1). Detailed results for all of the elements that were analyzed are available in Table S2.

We assessed the similarity of the sites based on a principal component analysis (PCA) of the following triplicated measurements: Total-Fe, SRO-Fe, Total-C, and texture (sand, silt, and clay) (Figure S3). We observed that ridges (R1, R2, R3) are grouped together, reflecting their difference in texture and Total-C content. Likewise, the slopes S1 and S2 could be grouped together based on their fine texture (clay and silt); however, S3 differs in its Fe characteristics. Valley sites V1, V2, and V3 were widely distributed across the different biplot quadrants (Figure S3), not only differing in the second principle component (V1, V2) from most of the ridge and slope sites, but also varying in texture and carbon content amongst themselves. Thus, each of the studied valleys had different characteristics, which may be reflected in the higher variation in Eh and other biogeochemical variables between the replicated valleys.

3.2. Precipitation and Environmental Factors Involved in Redox Processes

Over the course of the sampling period (May and June 2016), four distinct precipitation-related periods were identified (Figure 1): (1) intermittent rainfall periods of 5–10 mm every few days (from 3 May to 21 May 2016, phase-1); (2) a short absence of rain/dry period (from 21 May to 26 May 2016, phase-2); (3) an intense rainfall event of 290 mm for 10 days with a one-day event of 114 mm (from 27 May to 5 June 2016, phase-3); and (4) a longer dry period of 12 days (from 6 June to 17 June 2016, phase-4) with only one day of rain (26 mm). These patterns of precipitation directly influence the

variables that were measured hourly by the sensors (Eh, O_2, and θ_V) in most of the sites and catenas (Figures 2 and 3). θ_V fluctuated closely with precipitation in slope-1 and ridge-1. For example, in slope-1, θ_V decreased from 0.45 m^3 m^{-3} to 0.35 m^3 m^{-3} for the short dry period (phase-2), followed by an increase up to 0.47 m^3 m^{-3} in the intense rainfall event (phase-3), and decreased again to 0.36 m^3 m^{-3} in the long days without rain (phase-4). Valley-1 had a lower magnitude of soil moisture variation, as water appeared to remain longer in this landscape position (i.e., a poorly drained soil), from 0.45 m^3 m^{-3} to 0.50 m^3 m^{-3}. Soil O_2 did not fluctuate much for ridge-1 and slope-1, except for a slight change from 17.5% O_2 to 15.5% O_2 during phase-3. Valley-1 was more responsive to absences of precipitation than ridge-1 and slope-1, with O_2 increasing in valley-1 from 2.5% to 9.2% and 1.9% to 11.8% for the drying phase-2 and drying phase-4, respectively (Figure 2).

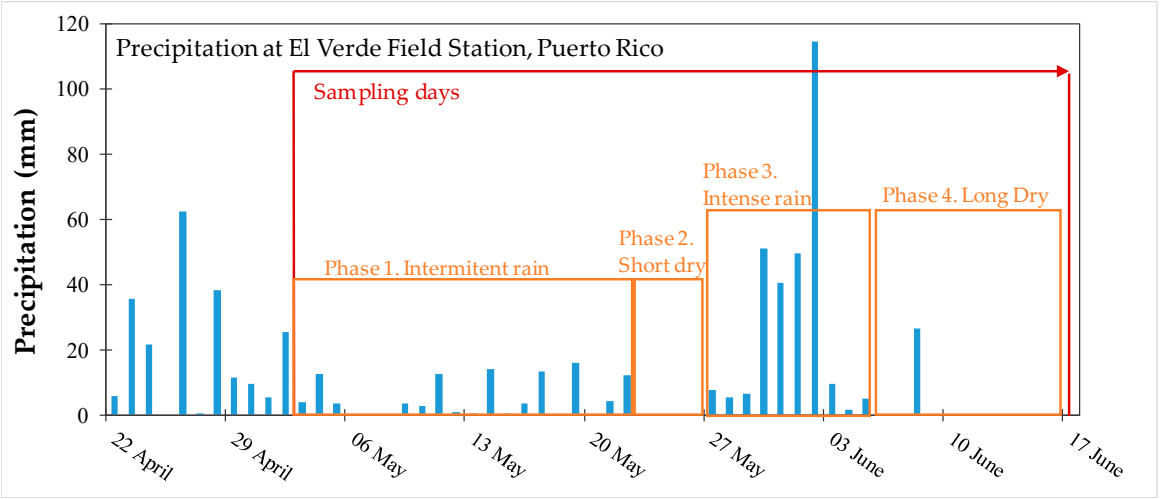

Figure 1. Phases identified during the sampling campaign, with precipitation at the El Verde Field Station, Puerto Rico. Phase-1: 3 May 2016 to 22 May 2016; phase-2: 23 May 2016 to 27 May 2016; phase-3: 28 May 2016 to 5 June 2016; and phase-4: 6 June 2016 to 17 June 2016.

Changes in redox potential had higher amplitude (magnitude) in the valley topographic positions compared to ridges and slopes. In valley-2 (catena-2), the four phases of precipitation (intermittent rain, no rain, intensive rain, and no rain again) were inversely correlated with the Eh (R^2 = 0.944) (Figure 3): Eh varied between from ~200 mV to ~500 mV within one to two days following rainfall (phase-1), increased from 325 mV to 550 mV during the short dry period (phase-2), and then decreased greatly from 550 mV to ~0 mV during the wet period (phase-3) before increasing back to 550 mV within the final drier days (phase-4). A notable redox fluctuation pattern also occurred in valley-3, with Eh reaching very negative values (from 260 mV to −360 mV) during the extreme rainfall event and returning to positive values (200 mV) for the long drier days. However, Eh in valley-1 (catena-1) remained mostly negative (−500 mV to −270 mV) due to high soil moisture (Figure 3). The Eh values that were measured in the three slopes and two ridges across all three catenas remained at values characteristic of oxic conditions (varying from 420 mV to 580 mV).

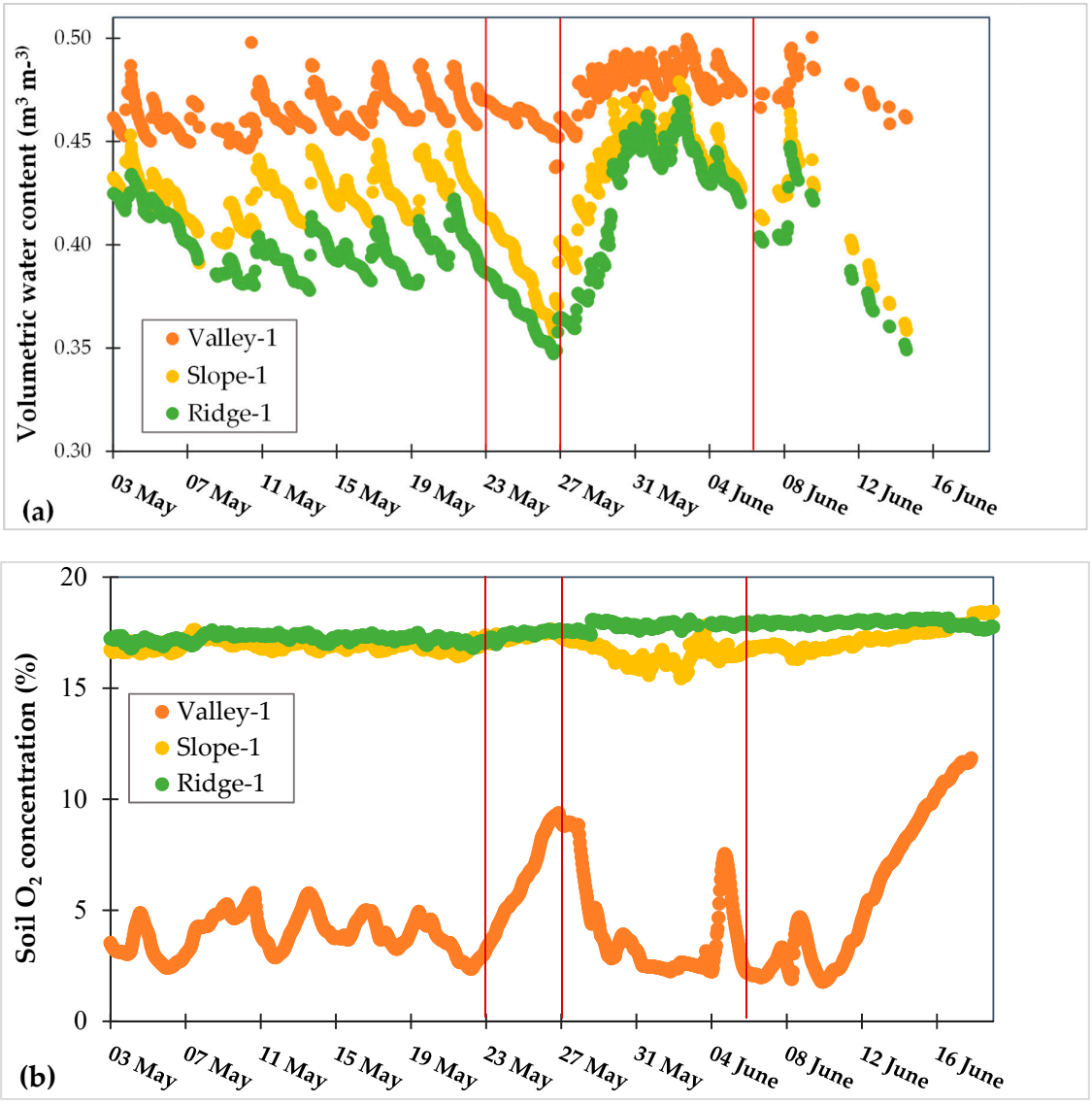

Figure 2. Soil volumetric water content (**a**) and oxygen (**b**). Red vertical lines separate the different phases of precipitation (phases 1, 2, 3, and 4).

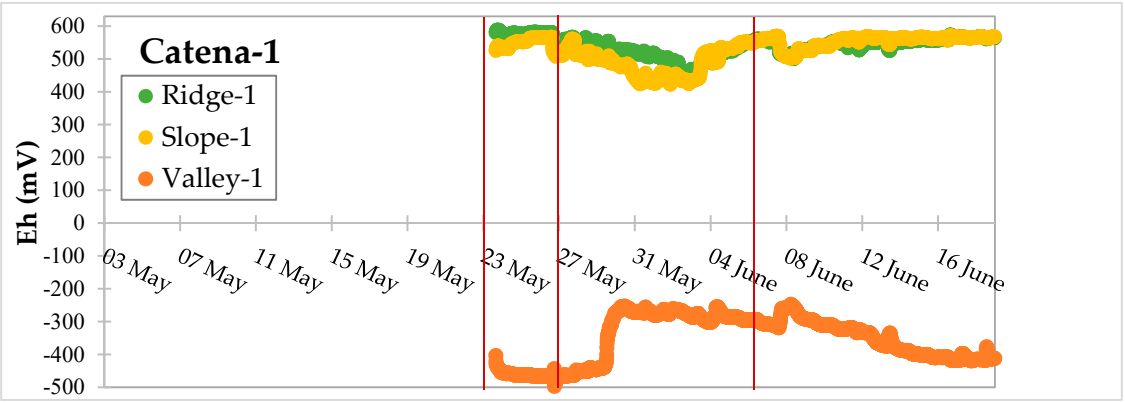

Figure 3. *Cont.*

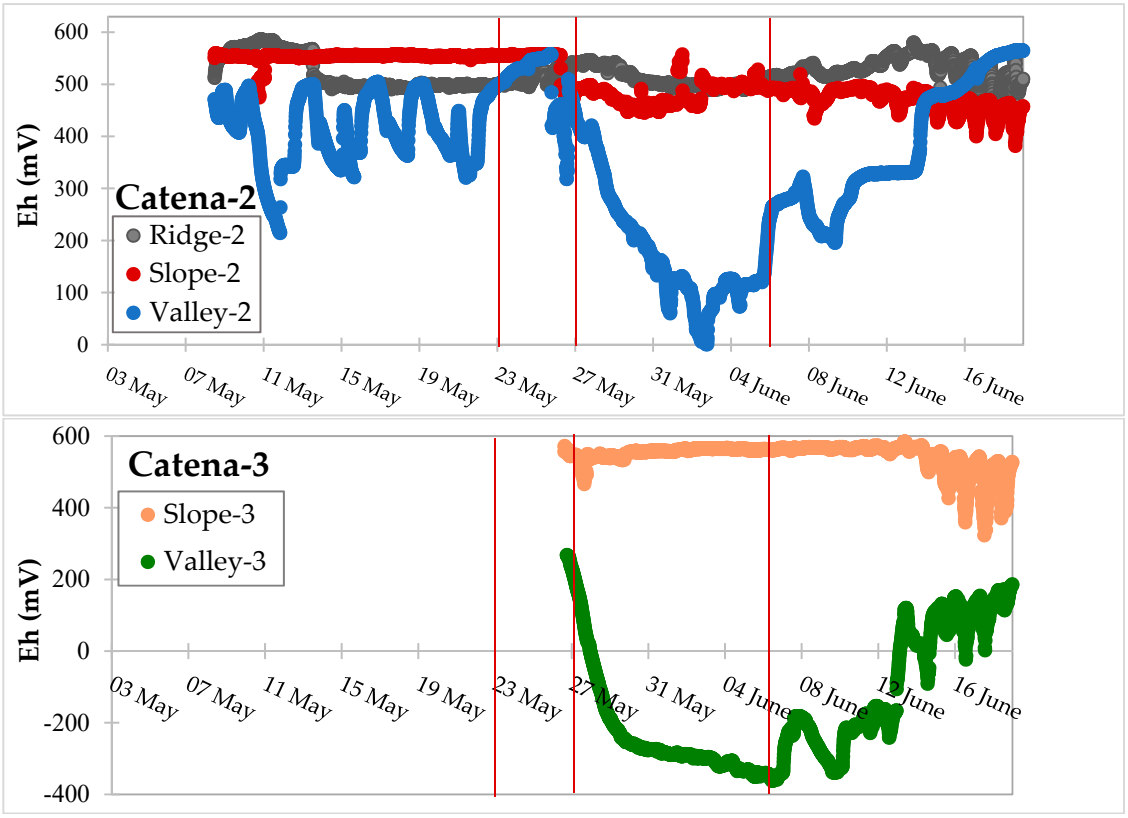

Figure 3. Redox potential (Eh) using platinum electrodes for each site within three catenas. Red vertical lines separate the different phases of precipitation (phases 1, 2, 3, and 4).

Using mixed-effects models with stepwise backwards elimination, daily average precipitation was identified as a significant predictor for the daily averages of Eh, O_2, and θ_V (negative, negative, and positive relationships; Table 2). We computed cross-correlations for the averaged daily measurements for the sensors, and we found no time lags between Eh, O_2, and θ_V.

Table 2. Summary of mixed-effect linear models for the environmental factors obtained by stepwise backwards elimination. All variables are daily averages.

Variable	Catenas	AIC [a] (R^2c) [b]	Num. of Observ. [c]	Model (Significant Predictors in Bold at $p < 0.05$)
Eh	All	3850.41 (0.944)	324	Eh = −0.7187 × **Precipitation**
O_2	1	866.20 (0.992)	240	O_2 = −0.0129 × **Precipitation**
θ_V	1	−880.34 (0.853)	213	$\theta_V = 4.894 \times 10^{-4}$ × **Precipitation**

[a] AIC: Akaike's information criterion; [b] R^2c: conditional R squared; [c] Maximum number of observations is 415 for all catenas and 243 for Catena 1 only. Units: Eh = deci-Volts, $\theta_V = m^3\ m^{-3}$, O_2 = %, and Precipitation = mm.

3.3. Dynamic Biogeochemical Soil Measurements

Soil extractions for Fe and C pools also varied over time in response to precipitation and soil moisture. HCl-extractable Fe^{II} varied across ridges to slopes to valleys for all three catenas (Figure 4). Valley-1 is wetter and had much higher Fe^{II} concentrations compared to all of the other sites in all of the catenas. During the 290-mm intense precipitation period (phase-3), the Fe^{II} in valley-1 varied from 50 mmol kg^{-1} to 126 mmol kg^{-1}. Ridge-2 and slope-2, particularly, had larger variation in Fe^{II} concentrations during phase-3 than the other ridges and slopes, where Fe^{II} content increased from 4 mmol kg^{-1} to 9 mmol kg^{-1} in ridge-2 and from 3 mmol kg^{-1} to 8 mmol kg^{-1} in slope-2. During the subsequent 12-day drying event (phase-4), Fe^{II} content decreased in most of the sites; for example, from 8 mmol kg^{-1} to 1 mmol kg^{-1} in slope-2, and from 4 mmol kg^{-1} to 1 mmol kg^{-1} in ridge-1 and ridge-2. Shewa-Fe^{III}_{RR} and Media-Fe^{III}_{RR} were also correlated with high or low rainfall

events and soil moisture contents varying overall from 1 mmol kg^{-1} to 50 mmol kg^{-1} soil day^{-1} (Figure 5). Shewa-Fe^{III}_{RR} was correlated with Media-Fe^{III}_{RR} (R^2 = 0.82), and both were correlated to Fe^{II} concentrations over the course of the experiment, which was consistent with the understanding that Fe^{III}_{RR} measurements assess the pool of Fe^{III} that can be rapidly reduced.

DOC did not fluctuate with precipitation (p = 0.610) as much as Eh and θ_V responded to precipitation. Across most of the sites, DOC remained near constant in the intense rainfall period (phase 3) and decreased in the last days of phase-4, with the exception of valley-1; for example, DOC declined from 264 mg kg^{-1} to 95 mg kg^{-1} in valley-3, and from 132 mg kg^{-1} to 114 mg kg^{-1} in slope-2 during the last drying event (Figure 6). Values of DOC were higher at some of the sampling points (e.g., maximum value of 275 mg kg^{-1} on 18 May 2016) for valley-1 than at the other sites, but they were still statistically similar to the DOC of the other sites across the 17 days of soil sampling, despite the higher values of Fe^{II} and Fe^{III}_{RR} pool in valley-1. The pH also did not clearly fluctuate in response to rainfall (p = 0.992) and soil moisture (p = 0.180) patterns (Figure S4). The pH (averaged over the 17 sampling days) was higher in the valleys, with values decreasing from 6.1 to 5.1 to 4.9 for valley-1, slope-1, and ridge-1, respectively. This increase in pH from ridge to slope to valley in catena-1 is associated with the greater amount of Fe^{II}, SRO-Fe, and total-C in valley-1. Acidic waterlogged soils commonly exhibit elevated pH due to the proton consumption during the reduction of nitrate, manganese, and iron [67].

Gravimetric water content (θ_G) was somewhat responsive to changes in precipitation (Figure S5). For example, in valley-2 gravimetric water content varied from 0.62 g g^{-1} to 0.84 g g^{-1} for the intense precipitation and decreased to 0.52 g g^{-1} over the next 12 days; however, the volumetric water content (measured hourly by sensors) captured the fluctuations in soil moisture in more detail. Fluxes of CO_2 were lower in valley-1 compared to slope-1 and ridge-1, with average values of 0.6 µmol m^{-2} s^{-1}, 1.6 µmol m^{-2} s^{-1}, and 1.3 µmol m^{-2} s^{-1} for each of these sites (Figure S6). Valley-1 was a source of CH_4, while slope-1 and ridge-1 were sinks of CH_4, with average CH_4 fluxes of 3.0 nmol m^{-2} s^{-1}, −5.6 nmol m^{-2} s^{-1}, and −0.4 nmol m^{-2} s^{-1}, respectively (Figure S6).

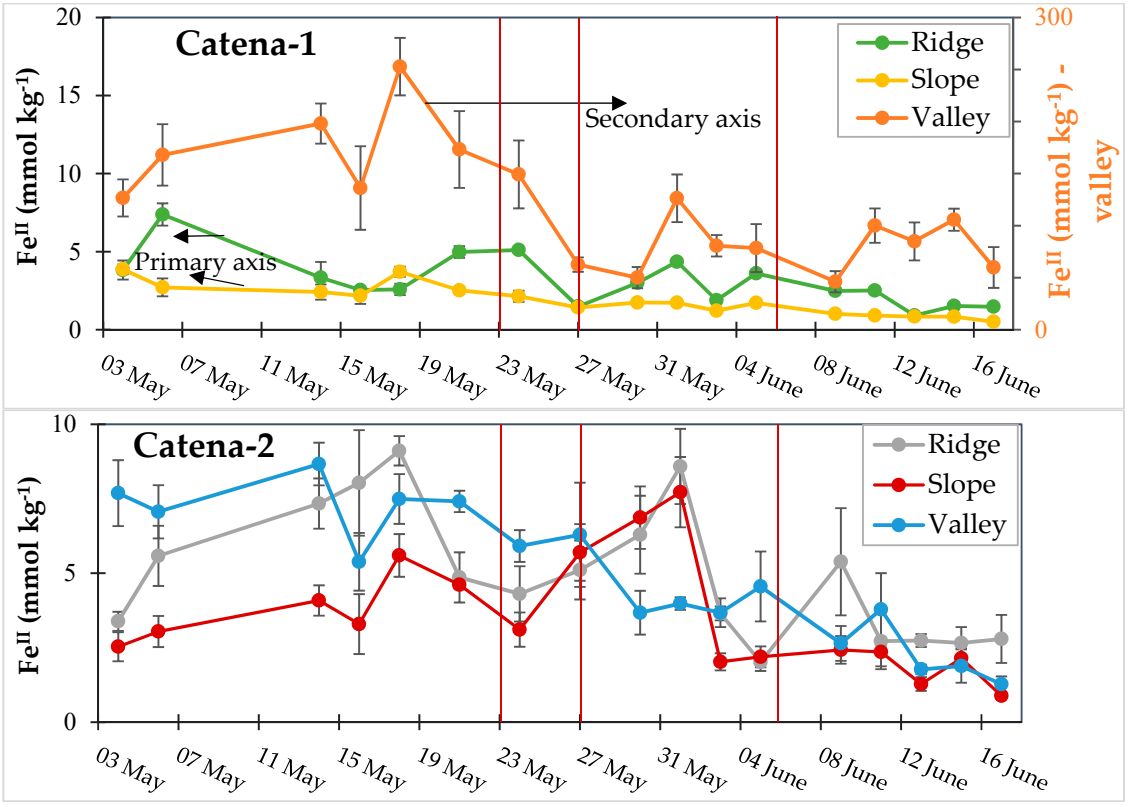

Figure 4. *Cont.*

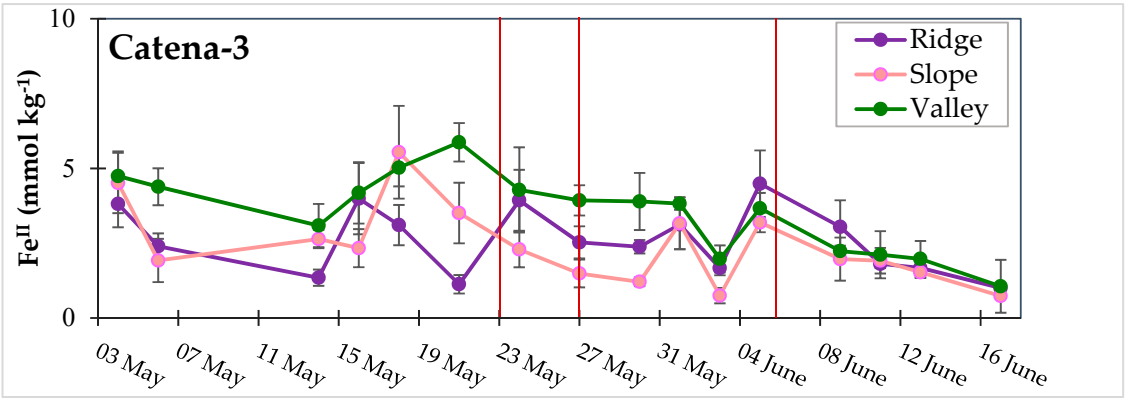

Figure 4. Fe^{II} at the ridge, slope, and valley for all three catenas. Error bars are ±1 SD. Red vertical lines separate the different phases of precipitation (phases 1, 2, 3, and 4).

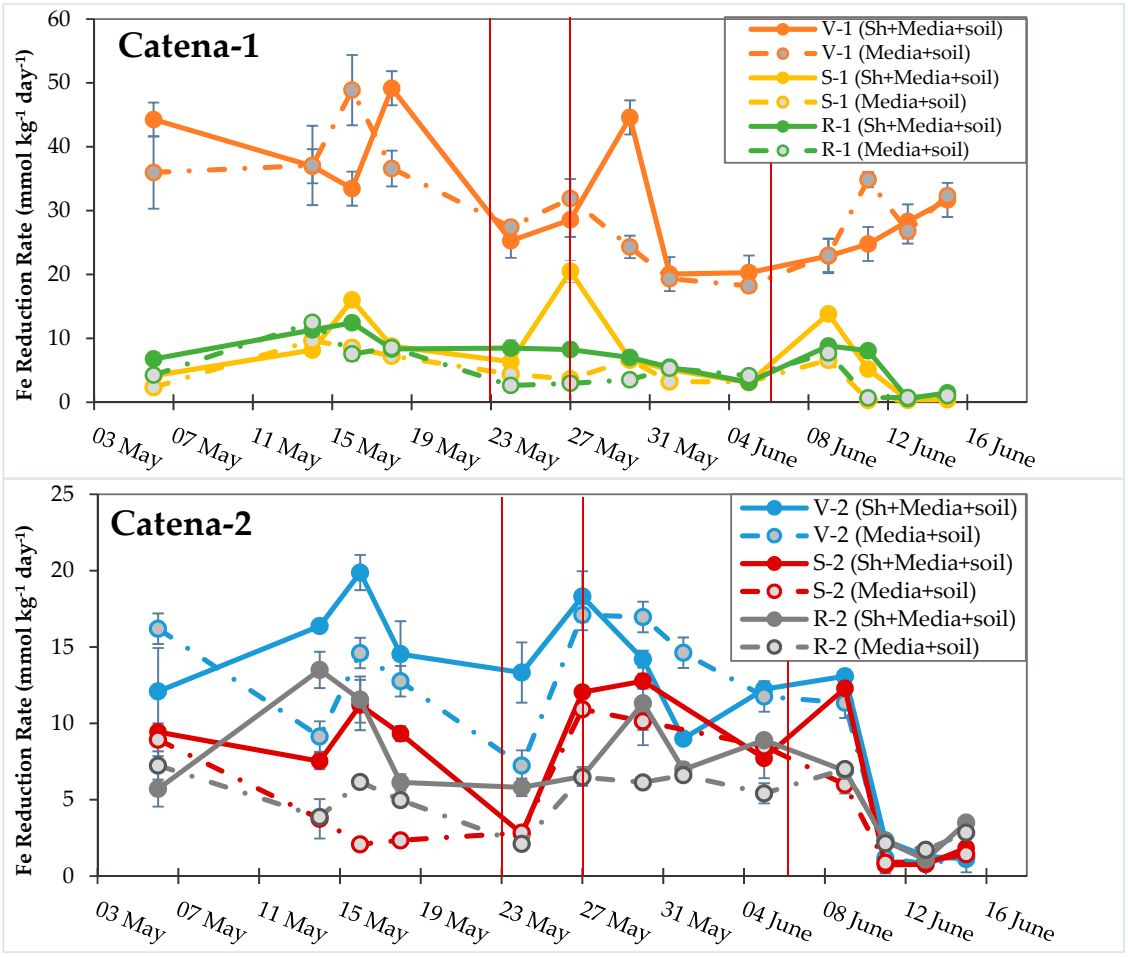

Figure 5. *Cont.*

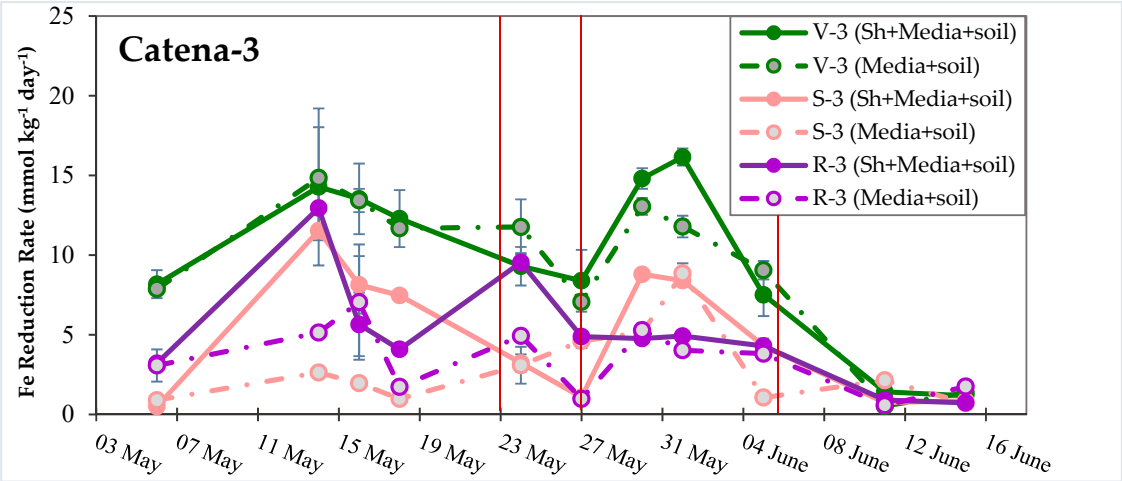

Figure 5. Soil Fe reduction rates (seven days) by Shewanella+media (Shewa-Fe^{III}_{RR}) or media only (Media-Fe^{III}_{RR}) incubations. Error bars are ±1 SD. Red vertical lines separate the different phases of precipitation (phases 1, 2, 3, and 4).

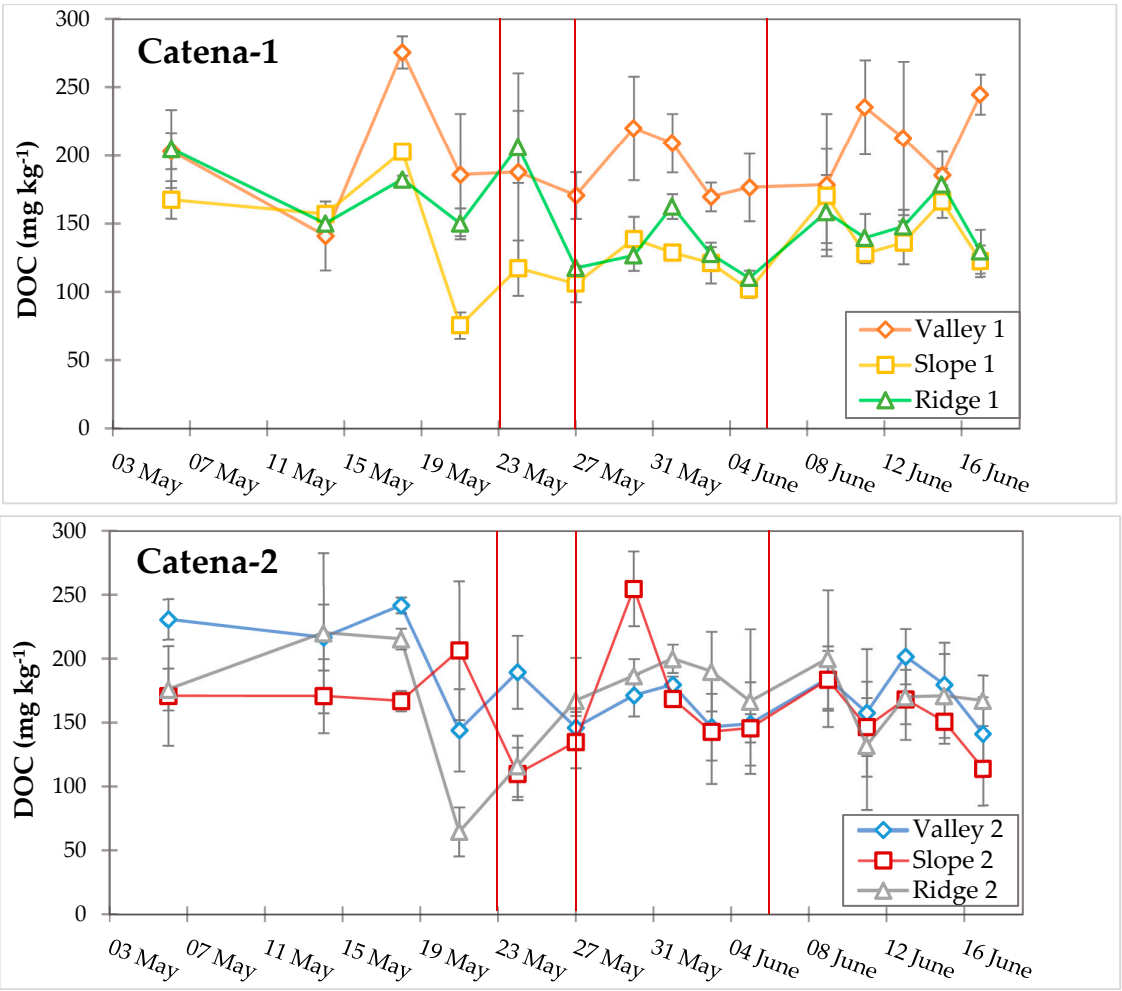

Figure 6. *Cont.*

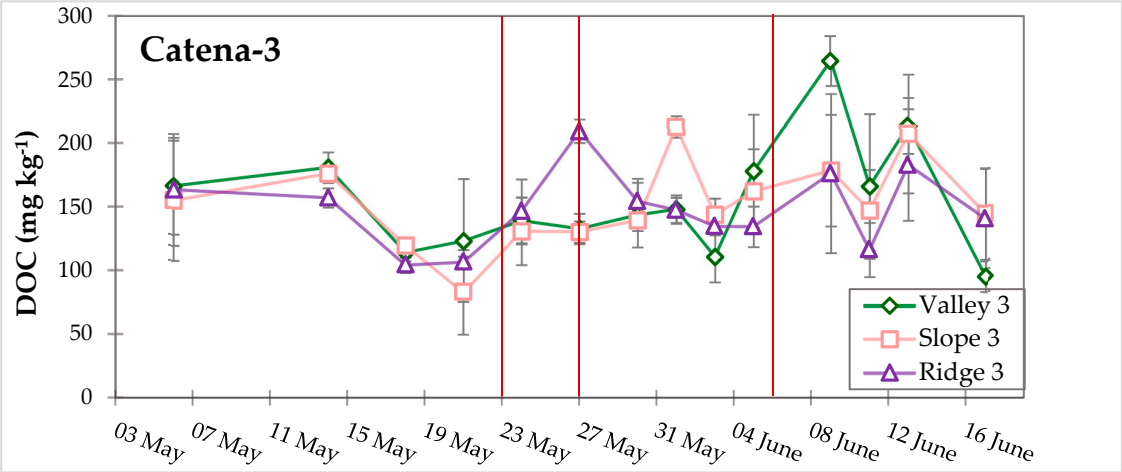

Figure 6. Dissolved organic carbon (DOC), 1:5 soil:water extraction. Error bars are ±1 SD. Red vertical lines separate the different phases of precipitation (Phases 1, 2, 3, and 4).

3.4. Turnover Timescales for HCl-Extractable Fe^{II} Pool and Statistical Models to Predict Soil Biogeochemical Parameters

Across all nine sites within the three catenas, the most common turnover time for the HCl-extractable Fe^{II} pool during net production was four days, and during the net HCl-extractable Fe^{II} consumption was three to four days; only in a few instances were longer turnover times measured (Figure 7, Table S3). We determined the optimal mixed-effects models for the biogeochemical variables Fe^{II}, Media-Fe^{III}_{RR}, Shewa-Fe^{III}_{RR}, DOC, F(CO_2), and F(CH_4) (Table 3) using stepwise backwards elimination, which removes all of the non-significant variables one by one, and keeps only the significant variables in the final elimination step (see initial parameters in Table S4). We chose the model with the lowest AIC (best model) by comparing the average of the measurements taken for Eh, O_2 and θ_V from 1 h, 2 h, 3 h, 6 h, 12 h, 24 h, 36 h, and 48 h preceding the time and date when the soil samples were taken. In the model predicting DOC concentration, the lowest AIC was the model with O_2 averaged over the preceding 48 h from the measurement (O_2_48 h) (Table S5). For precipitation, we used the two-day (or 48-h) averaged precipitation, which had the lowest AIC (Precipitation_48 h), compared to the averages of one, three, four, five, and 10 days prior to soil sampling. The two-day averaged precipitation was also found to be the time lag between the precipitation, the studied environmental factors, and biogeochemical variables.

Values of Fe^{III}_{RR} and pH were positively correlated with Fe^{II} levels for all of the catenas (all nine sites) (R^2 = 0.727), and O_2 was negatively correlated with Fe^{II} concentrations for the sites in catena-1 (Table 3) (R^2 = 0.789). We used Media-Fe^{III}_{RR} (and not Shewa-Fe^{III}_{RR}) for the Fe^{II} models, because Media-Fe^{III}_{RR} had the lowest AIC compared to Shewa-Fe^{III}_{RR} or both Media-Fe^{III}_{RR} and Shewa-Fe^{III}_{RR} together in the model. Gravimetric water content (θ_G) and Fe^{II} were positively correlated in both Media-Fe^{III}_{RR} and Shewa-Fe^{III}_{RR} models (R^2 = 0.835 and 0.810, respectively). Thus, Media-Fe^{III}_{RR} and Shewa-Fe^{III}_{RR} were indirectly driven by changes in precipitation. Eh was negatively correlated to Media-Fe^{III}_{RR}, and pH was positively correlated to Shewa-Fe^{III}_{RR} for all of the catenas (Table 3). DOC was positively correlated to θ_G and Fe^{II} (R^2 = 0.441). The F(CO_2) was negatively correlated to θ_V (Table 3) (R^2 = 0.429). For F(CH_4) models, we observed that the regression results were significantly impacted by five outlier values, and by removing these outliers, we observed a positive correlation of F(CH_4) and pH (Figure S7) (R^2 = 0.545).

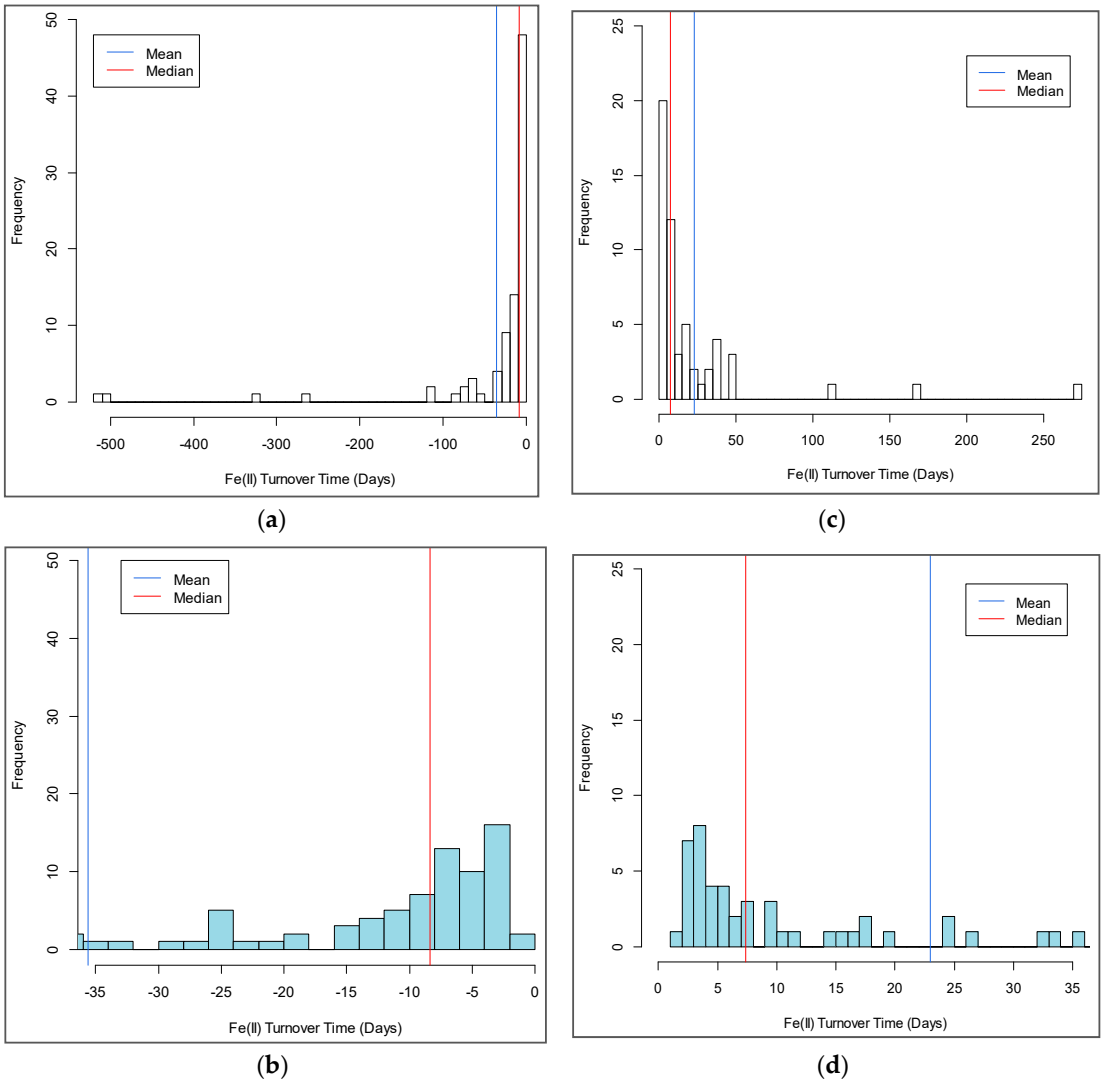

Figure 7. Turnover times for HCl-extractable Fe^{II} consumption (**a**,**b**) and Fe^{II} production (**c**,**d**) averaged for all sites. Figure (**b**,**d**) are equivalent to figure (**a**,**c**), respectively, but with tighter *x*-axis scales.

Table 3. Summary of mixed-effect linear models for the biogeochemical variables obtained by stepwise backwards elimination.

Variable	Catenas	AIC [a] (R^2c) [b]	Num. of Observ. [c]	Model (Significant Predictors in Bold at $p < 0.05$)
Fe^{II}	All	990.725 (0.727)	110	$Fe^{II} = 2.130 \times$ **Media-Fe^{III}_{RR}** $+ 20.286 \times$ **pH**
	Catena 1	377.89 (0.789)	39	$Fe^{II} = 2.4758 \times$ **Media-Fe^{III}_{RR}** $- 4.3644 \times$ **O_2_48 h**
Media-Fe^{III}_{RR}	All	413.32 (0.835)	73	Media-Fe^{III}_{RR} ~$0.1073 \times$ **Fe^{II}** $+ 20.295 \times$ **θ_G** $- 0.845 \times$ **Eh_6 h**
Shewa-Fe^{III}_{RR}	All	654.06 (0.810)	110	Shewa-Fe^{III}_{RR} ~$0.1202 \times$ **Fe^{II}** $+ 21.221 \times$ **θ_G** $+ 3.861 \times$ **pH**
DOC	All	718.68 (0.441)	132	DOC $= 0.1909 \times$ **Fe^{II}** $+ 12.47 \times$ **θ_G**
Flux CO_2	Catena 1	117.2 (0.429)	45	$F(CO_2) = -10.995 \times \theta_V$
Flux CH_4	Catena 1	126.01 (0.545)	43	$F(CH_4) = 2.782 \times$ **pH**

[a] AIC: Akaike's information criterion; [b] R^2c: conditional R squared; [c] Maximum number of observations is 153 for all catenas and 51 for Catena 1 only. Units: Fe^{II} = mmol kg^{-1}, Media-Fe^{III}_{RR} and Shewa-Fe^{III}_{RR} = mmol kg^{-1} d^{-1}, DOC = mg kg^{-1}; pH = unitless; θ_G = g g^{-1}; Eh = deci-Volts, θ_V = m^3 m^{-3}, O_2 = %, $F(CO_2)$ = µmol m^{-2} s^{-1}, and $F(CH_4)$ = nmol m^{-2} s^{-1}.

4. Discussion

4.1. Turnover Times for HCl-Extractable Fe^{II} Pool and Drivers of Fe Redox Processes

We aimed to measure the timescales for the turnover of the HCl-extractable Fe^{II} pool, in order to understand the controls on Fe^{II} biogeochemical cycling, and capture hot moments (of hours to days)

and identify hot spots for Fe cycling. Our field timeseries measurements revealed that HCl-extractable Fe^{II} turnover times that were calculated using consumption or production were centered around four days across ridges, slopes, and valleys. These results compare favorably to our prior controlled laboratory experiment [68], where the mean turnover for the HCl-extractable Fe^{II} pool that was calculated based on production varied from three to five days, and based on consumption from 0.5 to five days (this is likely faster than in the field because the laboratory experiments were slurry incubations). To our knowledge, there are no prior reports of Fe^{II} turnover times for soils under natural conditions, but turnover times can be calculated for some coastal marine systems [69–71]. For example, Wang and Van Cappellen [69] reported rates of dissimilatory Fe reduction and Fe^{II} concentrations (adsorbed Fe^{II} and $Fe^{II}CO_3$) for coastal marine sediments. From these values, we estimated that the turnover time for Fe^{II} pool was between 91–120 days. Thus, the Fe^{II} turnover according to these models are at least an order of magnitude longer than our results for the LEF soils, suggesting that these humid tropical soils exhibit rapid rates of Fe^{II} turnover.

Our mixed-effect models suggest that Fe reduction and oxidation, as measured by HCl-extracted Fe^{II} concentrations, are driven by O_2, pH, and the pool of rapidly reducible Fe^{III} oxides ($Fe^{III}{}_{RR}$). We interpret this correlation as follows. At the soil pH and O_2 content measured at the field sites, Fe^{II} concentrations are responsive to the pool of Fe^{III} oxides that are readily available for reduction, and are measured using either native soil microorganisms or via amendment with non-native bacteria (*Shewanella* sp.), the Media-$Fe^{III}{}_{RR}$ and Shewa-$Fe^{III}{}_{RR}$, respectively. Although soil moisture was not a predictor in the final Fe^{II} model, θ_G was a predictor for the rapidly reducible Fe^{III} oxides (Media-$Fe^{III}{}_{RR}$, in this case), which strongly impact the availability of Fe^{II} in soils. These findings corroborate our first hypothesis that precipitation is driving O_2 and soil moisture, and those parameters are in turn driving the $Fe^{III}{}_{RR}$ pool; thus, both O_2 and $Fe^{III}{}_{RR}$ control Fe^{II} concentrations, under the measured environmental conditions and soil pH at the field sites. So that, precipitation and soil moisture indirectly influenced Fe reduction and oxidation in soils from the LEF. These results agree with previous work demonstrating that a dissimilatory Fe reduction was controlled by environmental factors such as soil O_2 and water content, and the inherent soil Fe mineral composition [11,19,72].

In support of our second hypothesis that the valleys exhibit different Fe dynamics than other topographic positions, valley-1 contained much higher (and statistically different, $p < 0.05$) Fe^{II} concentrations (50 mmol kg^{-1} to 126 mmol kg^{-1}) and $Fe^{III}{}_{RR}$ rates (18 mmol kg^{-1} to 49 mmol kg^{-1} d^{-1}) than the other two valleys and all of the other ridges and slopes. However, for other biogeochemical variables, such as DOC, the values did not vary among the topographic positions. Thus, valley-1 was a hot spot for Fe biogeochemical processes compared to all other sites, and the other valleys (such as valley-2 and valley-3) may also generally serve as hot spots of Fe cycling.

To understand the redox processes across different landscape positions, complementary variables such as Eh, soil O_2, and bulk soil extractions for Fe^{II} (as an indicator of reducing conditions) can be used to assess the redox status of the environment. Eh measurements are suitable for soils that are consistently wet (such as the soil within valleys 1, 2, and 3). We observed a more pronounced variation in soil Eh in valley-2 and valley-3 than in valley-1, which followed similar trends in precipitation, soil moisture, and O_2 (valley-1 was constantly anoxic, with highly negative Eh values). Given the relatively constant negative Eh values in Valley-1, we investigated Eh models using only valley-2 and valley-3, which had greater variance in Eh in response to precipitation. In these analyses, we found a significant negative correlation ($p < 0.05$) between Fe^{II} and Eh. Thus, in some valley positions, the variations in redox potential (Eh) can be directly correlated with Fe reduction.

In our recent laboratory experiments incubating soil slurries from a similar valley topographic position in the LEF (Bisley watershed), we explored changes in Fe^{II} due to redox fluctuation parameters, such as the magnitude (or amplitude) of O_2, frequency/periodicity, and time length under oxic and anoxic conditions [18,49,73,74]. In these incubations, we found that the magnitude and periodicity of redox fluctuations influence Fe and C dynamics with clear patterns of Fe reduction during anoxia and Fe oxidation during oxic conditions. Indeed, the number of hours and days for the natural redox

fluctuations in valleys 2 and 3 (such as the notable changes in Eh), and the soil sampling periodicity we have done in the field, are comparable to the imposed 2.5 days, six days, and 10 days of anoxic conditions in the laboratory experiment [49].

4.2. The Dynamic Pool of Rapidly Reducible Fe Oxides (Fe^{III}_{RR})

We conducted soil incubations to assess the abundance of reactive Fe^{III} that is readily available for bacteria (Media-Fe^{III}_{RR} and Shewa-Fe^{III}_{RR}) as a bioreduction alternative to the selective chemical extractions such as citrate-ascorbate, oxalate, and hydroxylamine, e.g., Coward, et al. [75], Ginn, Meile, Wilmoth, Tang and Thompson [18], and Hall and Silver [35], which are generally thought to be static over month to year timescales. We found that both Media-Fe^{III}_{RR} and Shewa-Fe^{III}_{RR} were positively correlated with θ_G and Fe^{II}. Media-Fe^{III}_{RR} was negatively correlated with Eh, and Shewa-Fe^{III}_{RR} was positively correlated with pH. The observed values of Shewa-Fe^{III}_{RR} were generally similar to Media-Fe^{III}_{RR} values for valley-1 and valley-3. However, in the ridges and slopes, the values for Shewa-Fe^{III}_{RR} were generally higher than the values for Media-Fe^{III}_{RR}. These bioreduction results indicate that valleys can be nutrient and C-deficient for Fe reduction (as Fe^{III}_{RR} and SRO-Fe pools can be abundant), and slopes and ridges can be deficient in nutrients, C, and reactive Fe phases (Fe^{III}_{RR}) (Figure 5).

We found that both Shewa-Fe^{III}_{RR} and Media-Fe^{III}_{RR} changed in response to rainfall and soil moisture. For example, averaged over the 17 time points, Shewa-Fe^{III}_{RR} and Media-Fe^{III}_{RR} accounted for between 17–66 % and 12–64 % of the SRO-Fe pool, respectively, and reached a maximum value of ~100% of the SRO-Fe pool in some instances (Table S6). We also observed an overall increase in the Fe^{III}_{RR}/SRO-Fe ratio from ridges to slopes to valleys (Table S6). Thus, in our study, the valleys likely had a greater fraction of SRO-Fe that was readily available for use as an electron-acceptor (i.e., Fe^{III}_{RR}) relative to the slopes and ridges.

We propose that the pool of rapidly reducible Fe^{III} is a more dynamic and fluctuating pool than typically understood through selective extractions such as citrate-ascorbate or hydroxylamine [35,75]. While the full SRO-Fe pool as measured by these selective extractions may approximate the total amount of reducible Fe^{III}, this does not represent the Fe^{III} pool that can be reduced within short timescales, such as days and weeks. For instance, Ginn, Meile, Wilmoth, Tang and Thompson [18] observed that the SRO-Fe abundance was a poor predictor of Fe reduction rates, whereas measurements of Fe^{III}_{RR} via an incubation with an Fe-reducing microorganism were able to explain the difference in Fe reduction rates in the treatments. This rapidly reducible Fe^{III} pool (Fe^{III}_{RR}) is certainly a subset of the larger SRO. It likely comprises the least crystalline and most soluble portion of the SRO pool, but it may also be that it represents SRO Fe phases that are simply in closer proximity to the Fe-reducing organisms. The rapid oxidation of Fe^{II} results in Fe^{III} phases that are more reducible (and of lower crystallinity) than bulk Fe^{III} phases [73], but the presence of mineral surfaces and organic matter alter this crystallinity independent from the oxidation rate [30]. This suggests that frequent oxidation and reduction events may increase the proportion of Fe^{III}_{RR} relative to the total SRO-Fe pool. Our work here supports this hypothesis, but also suggests that the Fe^{III}_{RR} pool is quite dynamic and can vary considerably in response to multiple environmental forces. For example, in two distinct days of sampling for valley-1, the Fe^{III}_{RR} pool varied from 140 mmol kg^{-1} to 336 mmol kg^{-1}, reaching values as high as the SRO-Fe pool (Figure S8). In the latter case (higher Fe^{III}_{RR}), we would expect a soil primed for rapid and sustained Fe^{III} reduction, while in the former, the length of Fe reduction might be much lower (lower Fe^{III}_{RR}). Given the emerging understanding that Fe^{III} reduction is a critical electron-accepting process that is responsible for carbon mineralization in humid forest soils, the abundance of Fe^{III}_{RR} may be an important control of C-cycling.

4.3. Soil Moisture and Precipitation Influence Fe–C Redox Cycling

Soil moisture was a predictor for the Media-Fe^{III}_{RR}, Shewa-Fe^{III}_{RR}, DOC, and F(CO_2) models. Additionally, soil moisture influenced the Fe^{III}_{RR} pool, and consequently influenced Fe^{II} concentrations.

Precipitation was a predictor for the environmental factors Eh, O_2, and θ_V, which are important parameters that influence Fe–C reduction and oxidation (Figures 2 and 3). Prior work has shown that precipitation was inversely correlated with soil O_2 concentrations across the LEF [11]. By evaluating the relationship between precipitation and O_2, Liptzin, Silver and Detto [37] found that dry periods of at least four days were able to aerate soils, while a small rainfall event (<1 mm) was able to create low O_2 concentrations. We first hypothesized that precipitation would be a strong predictor for most of the soil biogeochemical variables. However, unlike soil moisture, precipitation did not prevail in the stepwise backward elimination models for Fe^{II}, Media-Fe^{III}_{RR}, Shewa-Fe^{III}_{RR}, DOC, $F(CO_2)$, and $F(CH_4)$. This suggests that rainfall does not have an immediate impact on Fe and C biogeochemistry, but rather it is the accumulation of water in the soil (soil moisture) that has a rapid impact on these parameters; reinforcing that soil moisture drives biogeochemical cycling, not rainfall. Additionally, elevated soil moisture content had a strong relationship with the potential for Fe reduction as measured by uniformly oxidized steel rods (i.e., Indicator of Reduction in Soils—IRIS) deployed across a topographic gradient in volcanic soils from Hawaii [76], and also in upland Fe-rich and weathered soils from the United States (USA) southeastern piedmont [77]. In these studies, Fe reduction was likely stimulated by exogenous C inputs (such as DOC). Therefore, the temporal and spatial variation in soil moisture, O_2 content, and redox conditions may create a hot moment for Fe reduction in soils within certain hot spots of the landscape [4,40].

In soils that undergo redox fluctuations, C has been shown to both accumulate in the form of solid phase C or be lost via solubilization or mineralization by soil microorganisms [78,79]. In our study, DOC was positively correlated to Fe^{II} and θ_G, suggesting that the release of DOC is likely driven by the desorption/dissolution of organic matter from reactive Fe^{III} phases that undergo reductive dissolution [80]. Consequently, DOC concentrations depend on the resident Fe reduction processes (as Fe^{II} is a predictive variable in the model for DOC) and on the soil moisture conditions. Our results corroborate prior work reporting that variations in DOC are correlated with changes in dissolved ferrous iron (Fe^{II}) [28,29]. During anoxic incubations of wetland soils, Grybos, et al. [81] observed that DOC increases were correlated with increases in pH as well as in Fe^{II} and Mn^{II} concentrations, and with decreases in Eh. These soluble C forms can be depolymerized and/or mineralized to CO_2 and CH_4 emissions by microbial activity [82]. In our models, we found that soil moisture was a predictor for $F(CO_2)$ and soil pH predictor for $F(CH_4)$; and, interestingly, we found no relationship between $F(CO_2)$ and $F(CH_4)$ with the iron pools Fe^{II} and Fe^{III}_{RR}. Similar to our models, other studies demonstrated that $F(CO_2)$ decreased with increasing soil moisture content [83–85], and that $F(CH_4)$ increased with increasing soil pH (between 4.5 to 6.5, Figure S7), for example, in inundated systems [86].

The decline in precipitation and soil moisture in the last 12 days of the field campaign correlated with a decrease in Fe^{II}, Fe^{III}_{RR}, DOC, and an increase in Eh and O_2 values at most of the sites. The decrease in both Fe^{II} and DOC concentrations could be due to the potential disappearance of anoxic microsites within the soils as the soil dried and O_2 content increased [4]. Thus, decreasing soil moisture conditions appeared to directly impact the dynamics of Fe and C with important ecosystem implications.

5. Conclusions

We found that variation in precipitation, soil moisture, and O_2 content impacted the pools of Fe and C extracted from soils across different landscape positions and influenced fluctuations in soil redox potential. The pool of reactive and rapidly reducible Fe oxides (Fe^{III}_{RR}) was dynamic and depended on fluctuating environmental conditions. We also found that the characteristic turnover time for HCl-extractable Fe^{II} (calculated based on both production and consumption) was four days. In conclusion, intensive periods of precipitation and prolonged dry periods were able to create distinct hot moments for biogeochemical redox processes. We found that valleys generally behaved as environmental hot spots within the landscape.

Robust relationships between soil moisture and the variables Media-Fe^{III}_{RR}, Shewa-Fe^{III}_{RR}, DOC, and CO_2 demonstrate the strong influence of soil water content on these biogeochemical processes. Both Media-Fe^{III}_{RR} and Shewa-Fe^{III}_{RR} were correlated to Fe^{II} concentrations in the studied soils. Thus, large amounts of precipitation or the occurrence of drier periods could likely further constrain these biogeochemical processes. We demonstrated that precipitation and the environmental factors of soil moisture and O_2 content are interconnected and important predictors for Fe reduction, DOC release, C mineralization, and fluctuations in soil redox potential, with important ecosystem implications over variant topographic positions in highly weathered Fe-rich soils from humid tropical regions.

Supplementary Materials: The following are available online at http://www.mdpi.com/2571-8789/2/4/59/s1, Figure S1: Illustration of sampling design at one of the catenas: (a) showing ridge, slope, and valley topographic positions, the 3 plots allocated within each site, the sensors distributed within the plots, and (b) example of a subplot of 1.5 m × 1.5 m, sampled at 0–15 cm depth with sampling points randomly located at least 20 cm apart. Luquillo CZO, Puerto Rico (2016), Figure S2: Visualization of subplots Catena-2: (a) slope, (b) ridge, and (c) valley; and (d) valley in Catena-3. Luquillo CZO, Puerto Rico (2016), Figure S3: Principal Component Analysis (PCA) for the 9 sites, valleys (V1, V2, V3), slopes (S1, S2, and S3), and ridges (R1, R2, R3) based on the following soil characteristics: Total-Fe, SRO-Fe, Total-C, Sand, Silt, and Clay content. Soils from Luquillo CZO, Puerto Rico, sampled in 2016, Figure S4: Soil pH (1:1 soil:water). Soils from Luquillo CZO, Puerto Rico, Figure S5: Gravimetric Water Content. Soils from Luquillo CZO, Puerto Rico, Figure S6. Soil CO2 and CH4 emissions. Soils from Luquillo CZO, Puerto Rico, Figure S7: Values for pH and CH_4 fluxes (a) with and (b) without the outliers, Figure S8: Pools of Total-Fe, SRO-Fe, Fe^{III}_{RR}, and Fe^{II} for two given sampling days (left and right) for valley-1. The pool of Fe^{III}_{RR} is dynamic and can be as high as the SRO-Fe pool. Soils from Luquillo CZO, Puerto Rico, sampled in 2016, Table S1: GPS coordinates of the studied site, Table S2: Total elemental analysis (concentrations in %). Soils from Luquillo CZO, Puerto Rico, sampled in 2016, Table S3: Turnover Times for HCl-extractable Fe^{II} Production and HCl-extractable Fe^{II} Consumption: highest frequency, median and mean, Table S4: Parameters used for each variable studied before stepwise backward elimination, Table S5: Number of hours before soil sampling the environmental factors are averaged that yielded the lowest AIC (best model). It represents the best averaging window to predict each variable in the mixed linear models (from 1 to 48 h of soil sampling), Table S6. Comparison of reactive iron pool (SRO-Fe) extracted by Citrate-Ascorbate and the Fe reduced within 7 days by incubations with Shewa-Fe^{III}_{RR} and Media-Fe^{III}_{RR}: (a) for the actual values in mmol kg^{-1} for the 7 day-incubation, and (b) for ratio between Fe^{III}_{RR} pool and the SRO-Fe pool (in percent).

Author Contributions: Conceptualization, D.B., C.S.O., W.S., A.T.; investigation, D.B., C.S.O., W.S., A.T., formal analysis, D.B., C.S.O., C.M., A.T.; data curation, D.B., C.M., A.T.; software, C.M.; funding acquisition, W.S., A.T.; supervision, A.T.; writing—review and editing, D.B., C.S.O., W.S., C.M., A.T.

Funding: Funding for this research was provided by National Science Foundation (NSF), grants EAR-1331841 and DEB-1457761.

Acknowledgments: We thank all members of the Thompson Lab (especially Nehru Mantripragada) for technical assistance. Thanks to the El Verde Research Station personal for providing support to this research (especially Francisco Perez), and to the Critical Zone Observatories Network.

Conflicts of Interest: The authors declare no conflict of interest.

References

1. Kleber, M.; Eusterhues, K.; Keiluweit, M.; Mikutta, C.; Mikutta, R.; Nico, P.S. Mineral–organic associations: Formation, properties, and relevance in soil environments. *Adv. Agron.* **2015**, *130*, 1–140.
2. FAO. Status of the World's Soil Resources (SWSR)–Main Report. In *Food and Agriculture Organization of the United Nations and Intergovernmental Technical Panel on Soils*; FAO: Rome, Italy, 2015; Volume 650.
3. Broedel, E.; Tomasella, J.; Cândido, L.A.; Randow, C. Deep soil water dynamics in an undisturbed primary forest in central Amazonia: Differences between normal years and the 2005 drought. *Hydrol. Process.* **2017**, *31*, 1749–1759. [CrossRef]
4. Hall, S.J.; McDowell, W.H.; Silver, W.L. When wet gets wetter: Decoupling of moisture, redox biogeochemistry, and greenhouse gas fluxes in a humid tropical forest soil. *Ecosystems* **2013**, *16*, 576–589. [CrossRef]
5. Saleska, S.R.; Miller, S.D.; Matross, D.M.; Goulden, M.L.; Wofsy, S.C.; Da Rocha, H.R.; De Camargo, P.B.; Crill, P.; Daube, B.C.; De Freitas, H.C. Carbon in Amazon forests: Unexpected seasonal fluxes and disturbance-induced losses. *Science* **2003**, *302*, 1554–1557. [CrossRef] [PubMed]

6. Álvarez-Dávila, E.; Cayuela, L.; González-Caro, S.; Aldana, A.M.; Stevenson, P.R.; Phillips, O.; Cogollo, Á.; Peñuela, M.C.; von Hildebrand, P.; Jiménez, E. Forest biomass density across large climate gradients in northern South America is related to water availability but not with temperature. *PLoS ONE* **2017**, *12*, e0171072. [CrossRef] [PubMed]
7. Brokaw, N.; Crowl, T.A.; Lugo, A.; McDowell, W.H.; Scatena, F.; Waide, R.B.; Willig, M.R. *A Caribbean Forest Tapestry: The Multidimensional Nature of Disturbance and Response*; Oxford University Press: New York, NY, USA, 2012.
8. Muggler, C.C.; van Griethuysen, C.; Buurman, P.; Pape, T. Aggregation, organic matter, and iron oxide morphology in Oxisols from Minas Gerais, Brazil. *Soil Sci.* **1999**, *164*, 759–770. [CrossRef]
9. Rezende, M.; Curi, N.; Rezende, S.; Corrêa, G. *Pedologia: Base Para Distinção de Ambientes*, 5th ed.; Editora UFLA: Lavras, Brazil, 2007; p. 322.
10. Cleveland, C. Nitrogen and phosphorus additions cause substantial losses of soil carbon from a lowland tropical rain forest. *Proc. Natl. Acad. Sci. USA* **2006**, *103*, 10316–10321. [CrossRef] [PubMed]
11. Silver, W.L.; Lugo, A.; Keller, M. Soil oxygen availability and biogeochemistry along rainfall and topographic gradients in upland wet tropical forest soils. *Biogeochemistry* **1999**, *44*, 301–328. [CrossRef]
12. Martin, S.T. Precipitation and dissolution of iron and manganese oxides. In *Environmental Catalysis*; CRC Press: Boca Raton, FL, USA, 2005; pp. 61–81.
13. Peters, V.; Conrad, R. Sequential reduction processes and initiation of CH4 production upon flooding of oxic upland soils. *Soil Biol. Biochem.* **1996**, *28*, 371–382. [CrossRef]
14. Hall, S.J.; Huang, W. Iron reduction: A mechanism for dynamic cycling of occluded cations in tropical forest soils? *Biogeochemistry* **2017**, *136*, 91–102. [CrossRef]
15. Lovley, D.R. Fe (III) and Mn (IV) reduction. In *Environmental Microbe-Metal Interactions*; American Society of Microbiology: Washington, DC, USA, 2000; pp. 3–30.
16. Mikutta, R.; Kleber, M.; Torn, M.S.; Jahn, R. Stabilization of soil organic matter: Association with minerals or chemical recalcitrance? *Biogeochemistry* **2006**, *77*, 25–56. [CrossRef]
17. Lugo, A.E.; Brown, S.; Brinson, M.M. Concepts in wetland ecology. *Ecosyst. World* **1990**, *15*, 53–85.
18. Ginn, B.; Meile, C.; Wilmoth, J.; Tang, Y.; Thompson, A. Rapid Iron Reduction Rates Are Stimulated by High-Amplitude Redox Fluctuations in a Tropical Forest Soil. *Environ. Sci. Technol.* **2017**, *51*, 3250–3259. [CrossRef]
19. Weber, K.A.; Achenbach, L.A.; Coates, J.D. Microorganisms pumping iron: Anaerobic microbial iron oxidation and reduction. *Nat. Rev. Microbiol.* **2006**, *4*, 752–764.
20. Cornell, R.M.; Schwertmann, U. *The Iron Oxides: Structure, Properties, Reactions, Occurrences and Uses*; Wiley-VCH: Weinheim, Germany, 2003; p. 667.
21. Neff, J.C.; Asner, G.P. Dissolved organic carbon in terrestrial ecosystems: Synthesis and a model. *Ecosystems* **2001**, *4*, 29–48. [CrossRef]
22. Gottschalk, P.; Smith, J.U.; Wattenbach, M.; Bellarby, J.; Stehfest, E.; Arnell, N.; Osborn, T.; Jones, C.; Smith, P. How will organic carbon stocks in mineral soils evolve under future climate? Global projections using RothC for a range of climate change scenarios. *Biogeosciences* **2012**, *9*, 3151. [CrossRef]
23. Lovley, D.R.; Holmes, D.E.; Nevin, K.P. Dissimilatory fe (iii) and mn (iv) reduction. *Adv. Microb. Physiol.* **2004**, *49*, 219–286. [PubMed]
24. Carmo, J.B.D.; Keller, M.; Dias, J.D.; Camargo, P.B.D.; Crill, P. A source of methane from upland forests in the Brazilian Amazon. *Geophys. Res. Lett.* **2006**, *33*. [CrossRef]
25. Rasmussen, C.; Throckmorton, H.; Liles, G.; Heckman, K.; Meding, S.; Horwath, W. Controls on Soil Organic Carbon Partitioning and Stabilization in the California Sierra Nevada. *Soil Syst.* **2018**, *2*, 41.
26. Huang, W.; Hall, S.J. Elevated moisture stimulates carbon loss from mineral soils by releasing protected organic matter. *Nat. Commun.* **2017**, *8*, 1774.
27. Hall, S.J.; Silver, W.L. Iron oxidation stimulates organic matter decomposition in humid tropical forest soils. *Glob. Chang. Biol.* **2013**, *19*, 2804–2813. [CrossRef] [PubMed]
28. Knorr, K.-H. DOC-dynamics in a small headwater catchment as driven by redox fluctuations and hydrological flow paths-are DOC exports mediated by iron reduction/oxidation cycles? *Biogeosciences* **2013**, *10*, 891. [CrossRef]
29. Blodau, C.; Fulda, B.; Bauer, M.; Knorr, K.-H. Arsenic speciation and turnover in intact organic soil mesocosms during experimental drought and rewetting. *Geochim. Cosmochim. Acta* **2008**, *72*, 3991–4007. [CrossRef]

30. Chen, C.; Thompson, A. Ferrous Iron Oxidation under Varying pO2 Levels: The Effect of Fe (III)/Al (III) Oxide Minerals and Organic Matter. *Environ. Sci. Technol.* **2018**, *52*, 597–606. [CrossRef] [PubMed]
31. Thaymuang, W.; Kheoruenromne, I.; Suddhipraharn, A.; Sparks, D.L. The role of mineralogy in organic matter stabilization in tropical soils. *Soil Sci.* **2013**, *178*, 308–315. [CrossRef]
32. Souza, I.F.; Almeida, L.F.; Jesus, G.L.; Pett-Ridge, J.; Nico, P.S.; Kleber, M.; Silva, I.R. Carbon Sink Strength of Subsurface Horizons in Brazilian Oxisols. *Soil Sci. Soc. Am. J.* **2018**, *82*, 76–86. [CrossRef]
33. Silva, L.C.; Doane, T.A.; Corrêa, R.S.; Valverde, V.; Pereira, E.I.; Horwath, W.R. Iron-mediated stabilization of soil carbon amplifies the benefits of ecological restoration in degraded lands. *Ecol. Appl.* **2015**, *25*, 1226–1234. [CrossRef] [PubMed]
34. Silva Neto, L.F.; Vasconcellos Inda, A.; Bayer, C.; Pinheiro Dick, D.; Tiago Tonin, A. Óxidos de ferro em latossolos tropicais e subtropicais brasileiros em plantio direto. *Rev. Bras. Ciênc. Solo* **2008**, *32*, 1873–1881. [CrossRef]
35. Hall, S.J.; Silver, W.L. Reducing conditions, reactive metals, and their interactions can explain spatial patterns of surface soil carbon in a humid tropical forest. *Biogeochemistry* **2015**, *125*, 149–165. [CrossRef]
36. O'Connell, C.S.; Ruan, L.; Silver, W.L. Drought drives rapid shifts in tropical rainforest soil biogeochemistry and greenhouse gas emissions. *Nat. Commun.* **2018**, *9*, 1348. [CrossRef] [PubMed]
37. Liptzin, D.; Silver, W.L.; Detto, M. Temporal Dynamics in Soil Oxygen and Greenhouse Gases in Two Humid Tropical Forests. *Ecosystems* **2011**, *14*, 171–182. [CrossRef]
38. Hook, P.B.; Burke, I.C. Biogeochemistry in a shortgrass landscape: Control by topography, soil texture, and microclimate. *Ecology* **2000**, *81*, 2686–2703.
39. Bernhardt, E.S.; Blaszczak, J.R.; Ficken, C.D.; Fork, M.L.; Kaiser, K.E.; Seybold, E.C. Control points in ecosystems: Moving beyond the hot spot hot moment concept. *Ecosystems* **2017**, *20*, 665–682. [CrossRef]
40. McClain, M.E.; Boyer, E.W.; Dent, C.L.; Gergel, S.E.; Grimm, N.B.; Groffman, P.M.; Hart, S.C.; Harvey, J.W.; Johnston, C.A.; Mayorga, E. Biogeochemical hot spots and hot moments at the interface of terrestrial and aquatic ecosystems. *Ecosystems* **2003**, *6*, 301–312. [CrossRef]
41. Vargas, R.; Sánchez-Cañete, P.E.; Serrano-Ortiz, P.; Curiel Yuste, J.; Domingo, F.; López-Ballesteros, A.; Oyonarte, C. Hot-Moments of Soil CO_2 Efflux in a Water-Limited Grassland. *Soil Syst.* **2018**, *2*, 47. [CrossRef]
42. Seiders, V.M. Cretaceous and Lower Tertiary Stratigraphy of the Gurabo and El Yunque Quadrangles, Puerto Rico. 1971. Available online: http://agris.fao.org/agris-search/search.do?recordID=US201300472921 (accessed on 14 June 2017).
43. Hodge, E.T. *Geology of the Coamo-Guayama District*; New York Academy of Sciences: New York, NY, USA, 1920; Volume 28.
44. Heartsill-Scalley, T.; Scatena, F.N.; Estrada, C.; McDowell, W.; Lugo, A.E. Disturbance and long-term patterns of rainfall and throughfall nutrient fluxes in a subtropical wet forest in Puerto Rico. *J. Hydrol.* **2007**, *333*, 472–485. [CrossRef]
45. Scatena, F.N. *An Introduction to the Physiography and History of the Bisley Experimental Watersheds in the Luquillo Mountains of Puerto Rico*; Gen. Tech. Report SO-72; US Department of Agriculture, Forest Service, Southern Forest Experiment Station: New Orleans, LA, USA, 1989; Volume 72.
46. Almaraz, M. Nitrogen Availability and Loss from Unmanaged and Managed Ecosystems. Ph.D. Thesis, Brown University, Providence, RI, USA, 2017.
47. McDowell, W.; Estrada-Pinto, A. *Rainfall at the El Verde Field Station, 1964–1986*; CEER T-228; University of Puerto Rico: San Juan, Puerto Rico, 1988.
48. Ginn, B.R.; Habteselassie, M.Y.; Meile, C.; Thompson, A. Effects of sample storage on microbial Fe-reduction in tropical rainforest soils. *Soil Biol. Biochem.* **2014**, *68*, 44–51. [CrossRef]
49. Barcellos, D.; Cyle, K.T.; Thompson, A. Faster redox fluctuations can lead to higher iron reduction rates in humid forest soils. *Biogeochemistry* **2018**, *137*, 367–378. [CrossRef]
50. Thompson, A.; Chadwick, O.A.; Rancourt, D.G.; Chorover, J. Iron-oxide crystallinity increases during soil redox oscillations. *Geochim. Cosmochim. Acta* **2006**, *70*, 1710–1727. [CrossRef]
51. Huang, W.; Hall, S.J. Optimized high-throughput methods for quantifying iron biogeochemical dynamics in soil. *Geoderma* **2017**, *306*, 67–72. [CrossRef]
52. Haynes, R.; Francis, G. Changes in microbial biomass C, soil carbohydrate composition and aggregate stability induced by growth of selected crop and forage species under field conditions. *Eur. J. Soil Sci.* **1993**, *44*, 665–675. [CrossRef]

53. Boyer, J.; Groffman, P. Bioavailability of water extractable organic carbon fractions in forest and agricultural soil profiles. *Soil Biol. Biochem.* **1996**, *28*, 783–790. [CrossRef]
54. Ghani, A.; Dexter, M.; Perrott, K. Hot-water extractable carbon in soils: A sensitive measurement for determining impacts of fertilisation, grazing and cultivation. *Soil Biol. Biochem.* **2003**, *35*, 1231–1243. [CrossRef]
55. Guigue, J.; Mathieu, O.; Lévêque, J.; Mounier, S.; Laffont, R.; Maron, P.-A.; Navarro, N.; Chateau, C.; Amiotte-Suchet, P.; Lucas, Y. A comparison of extraction procedures for water-extractable organic matter in soils. *Eur. J. Soil Sci.* **2014**, *65*, 520–530. [CrossRef]
56. Pachon, J.C.; Kowalski, K.; Butterick, J.; Bacon, A.R. The quantified effect of real refractive index assumptions on laser diffraction mechanical analysis. *Soil Sci. Soc. Am. J.* **2018**, in press.
57. Bonneville, S.; Van Cappellen, P.; Behrends, T. Microbial reduction of iron (III) oxyhydroxides: Effects of mineral solubility and availability. *Chem. Geol.* **2004**, *212*, 255–268. [CrossRef]
58. Bonneville, S.; Behrends, T.; Van Cappellen, P. Solubility and dissimilatory reduction kinetics of iron (III) oxyhydroxides: A linear free energy relationship. *Geochim. Cosmochim. Acta* **2009**, *73*, 5273–5282. [CrossRef]
59. Eusterhues, K.; Hädrich, A.; Neidhardt, J.; Küsel, K.; Keller, T.; Jandt, K.; Totsche, K. Reduction of ferrihydrite with adsorbed and coprecipitated organic matter: Microbial reduction by Geobacter bremensis vs. abiotic reduction by Na-dithionite. *Biogeosciences* **2014**, *11*, 4953. [CrossRef]
60. Fiedler, S.; Vepraskas, M.J.; Richardson, J. Soil redox potential: Importance, field measurements, and observations. *Adv. Agron.* **2007**, *94*, 1–54.
61. Husson, O. Redox potential (Eh) and pH as drivers of soil/plant/microorganism systems: A transdisciplinary overview pointing to integrative opportunities for agronomy. *Plant Soil* **2013**, *362*, 389–417. [CrossRef]
62. Patrick, W.; Gambrell, R.; Faulkner, S. Redox measurements of soils. In *Methods of Soil Analysis Part 3—Chemical Methods*; Soil Science Society of America: Madison, WI, USA, 1996; pp. 1255–1273.
63. Sparks, D.L. *Environmental Soil Chemistry*; Academic Press: San Diego, CA, USA, 2003; p. 351.
64. Bates, D.; Mächler, M.; Bolker, B.; Walker, S. Fitting linear mixed-effects models using lme4. *arXiv* **2014**.
65. Johnson, P.C. Extension of Nakagawa & Schielzeth's R2GLMM to random slopes models. *Methods Ecol. Evol.* **2014**, *5*, 944–946. [PubMed]
66. Nakagawa, S.; Schielzeth, H. A general and simple method for obtaining R2 from generalized linear mixed-effects models. *Methods Ecol. Evol.* **2013**, *4*, 133–142. [CrossRef]
67. Ponnamperuma, F.N. The chemistry of submerged soils. *Adv. Agron.* **1972**, *24*, 29–96.
68. Barcellos, D. Biogeochemical Cycling of Iron and Carbon in Humid (Sub)tropical Forest Soils under Fluctuating Redox Conditions. Ph.D. Thesis, University of Georgia, Athens, GA, USA, 2018.
69. Wang, Y.; Van Cappellen, P. A multicomponent reactive transport model of early diagenesis: Application to redox cycling in coastal marine sediments. *Geochim. Cosmochim. Acta* **1996**, *60*, 2993–3014. [CrossRef]
70. Berg, P.; Rysgaard, S.; Thamdrup, B. Dynamic modeling of early diagenesis and nutrient cycling. A case study in an artic marine sediment. *Am. J. Sci.* **2003**, *303*, 905–955. [CrossRef]
71. Boudreau, B.P. A method-of-lines code for carbon and nutrient diagenesis in aquatic sediments. *Comput. Geosci.* **1996**, *22*, 479–496. [CrossRef]
72. Hall, S.J.; Liptzin, D.; Buss, H.L.; DeAngelis, K.; Silver, W.L. Drivers and patterns of iron redox cycling from surface to bedrock in a deep tropical forest soil: A new conceptual model. *Biogeochemistry* **2016**, *130*, 177–190. [CrossRef]
73. Chen, C.; Meile, C.; Wilmoth, J.; Barcellos, D.; Thompson, A. Influence of PO_2 on Iron Redox Cycling and Anaerobic Organic Carbon Mineralization in a Humid Tropical Forest Soil. *Environ. Sci. Technol.* **2018**, *52*, 7709–7719. [CrossRef] [PubMed]
74. Wilmoth, J.L.; Moran, M.A.; Thompson, A. Transient O_2 pulses direct Fe crystallinity and Fe(III)-reducer gene expression within a soil microbiome. *Microbiome* **2018**, *6*, 189. [CrossRef] [PubMed]
75. Coward, E.K.; Thompson, A.T.; Plante, A.F. Iron-mediated mineralogical control of organic matter accumulation in tropical soils. *Geoderma* **2017**, *306*, 206–216. [CrossRef]
76. Hodges, C.; King, E.; Pett-Ridge, J.; Thompson, A. Potential for Iron Reduction Increases with Rainfall in Montane Basaltic Soils of Hawaii. *Soil Sci. Soc. Am. J.* **2018**, *82*, 176–185. [CrossRef]
77. Hodges, C.A. Drivers and Variability of Iron Reduction in Upland Soils. Master's Thesis, University of Georgia, Athens, GA, USA, 2017.

78. Kögel-Knabner, I. The macromolecular organic composition of plant and microbial residues as inputs to soil organic matter: Fourteen years on. *Soil Biol. Biochem.* **2017**, *105*, A3–A8. [CrossRef]
79. Six, J.; Conant, R.; Paul, E.; Paustian, K. Stabilization mechanisms of soil organic matter: Implications for C-saturation of soils. *Plant Soil* **2002**, *241*, 155–176. [CrossRef]
80. Buettner, S.W.; Kramer, M.G.; Chadwick, O.A.; Thompson, A. Mobilization of colloidal carbon during iron reduction in basaltic soils. *Geoderma* **2014**, *221*, 139–145. [CrossRef]
81. Grybos, M.; Davranche, M.; Gruau, G.; Petitjean, P.; Pédrot, M. Increasing pH drives organic matter solubilization from wetland soils under reducing conditions. *Geoderma* **2009**, *154*, 13–19. [CrossRef]
82. Keiluweit, M.; Nico, P.S.; Kleber, M.; Fendorf, S. Are oxygen limitations under recognized regulators of organic carbon turnover in upland soils? *Biogeochemistry* **2016**, *127*, 157–171. [CrossRef]
83. Manabe, S.; Wetherald, R.T. Reduction in summer soil wetness induced by an increase in atmospheric carbon dioxide. *Science* **1986**, *232*, 626–628. [CrossRef] [PubMed]
84. Davidson, E.A.; Belk, E.; Boone, R.D. Soil water content and temperature as independent or confounded factors controlling soil respiration in a temperate mixed hardwood forest. *Glob. Chang. Biol.* **1998**, *4*, 217–227. [CrossRef]
85. Xu, M.; Qi, Y. Soil-surface CO_2 efflux and its spatial and temporal variations in a young ponderosa pine plantation in northern California. *Glob. Chang. Biol.* **2001**, *7*, 667–677. [CrossRef]
86. Wang, Z.; Delaune, R.; Patrick, W.; Masscheleyn, P. Soil redox and pH effects on methane production in a flooded rice soil. *Soil Sci. Soc. Am. J.* **1993**, *57*, 382–385. [CrossRef]